Pergamon
www.elsevier.com/locate/pnucene

Progress in Nuclear Energy, Vol. 39, No. 2, pp. 119–144, 2001

Printed in Great Britain
0149-1970/01/$ - see front matter

PII: S0149-1970(01)00007-5

3D RADIATION TRANSPORT BENCHMARK PROBLEMS AND RESULTS FOR SIMPLE GEOMETRIES WITH VOID REGION

KEISUKE KOBAYASHI* and NAOKI SUGIMURA†

Department of Nuclear Engineering, Kyoto University
Yoshida, Sakyoku, Kyoto, Japan
kobayasi@ip.media.kyoto-u.ac.jp
naoki_sugimura@gijutsu.neltd.co.jp

YASUNOBU NAGAYA

Department of Nuclear Energy System
Japan Atomic Energy Research Institute
Tokai-mura, Naka-gun, Ibaraki, Japan
nagaya@mike.tokai.jaeri.go.jp

Abstract — Three-dimensional (3D) transport benchmark problems for simple geometries with void region were proposed at the OECD/NEA in order to check the accuracy of deterministic 3D transport programs. The exact total fluxes by the analytical method are given for the pure absorber cases, and Monte Carlo values are given for the 50% scattering cases as the reference values. The total fluxes of all contributions to the present benchmark problems calculated by the 3D transport programs, TORT, TORT with FNSUNCL3, PARTISN, PENTRAN, IDT, MCCG3D, EVENT and ARDRA are compared in figures.

Keywords: 3D Transport Calculations; Benchmark Problems; Benchmark Results; Void Problems

1 INTRODUCTION

In the OECD proceedings on 3D deterministic radiation transport computer programs edited by Sartori (1997), many 3D deterministic transport programs were presented. It is not simple, however, to determine their special features or their accuracy. One of the difficulties in multi-dimensional transport calculations concerns the accuracy of the flux distribution for systems which have void regions in a highly absorbing medium.

The method which is most widely used to solve the 3D transport equation is the discrete ordinates method. However, this method has the disadvantage of the ray effect and we must be cautious which S_n order and which quadrature set for the angular discretization should be used for such systems. On the other hand, the spherical harmonics method has the advantage of causing no ray effect, but

*Present status: Emeritus Professor of Kyoto University
†Present address: Nuclear Engineering Co., Tosabori 1-3-7, Nishiku, Osaka

the equations are very complicated and it is difficult to derive the finite difference or discrete equations which satisfy the necessary boundary conditions at material interfaces as discussed by Kobayashi (1995). Then, the flux distribution by the spherical harmonics method shows some anomalies at the material interfaces of large cross section differences or at the material void interface. This was seen in the flux distribution of the 3D benchmark calculations with void region proposed by Takeda (1991), where appreciable discrepancies were observed in the flux distribution between programs based on the spherical harmonics method as shown by Kobayashi (1995).

Ackroyd and Riyait (1989) investigated flux distributions for 2D void problems extensively, and their results show that these void problems are really difficult which suggests that 3D transport programs should also be checked for these problems.

The 3D benchmark void problems of simple geometries were proposed at the OECD/NEA in 1996 by Kobayashi (1997) which were simple extensions of the 2D void problems given by Ackroyd and Riyait to 3D geometries. There are two kinds of one-group source problems. One is a system of a pure absorber with a void region so that the exact solution can be obtained by numerical integration. The other one has the same geometry as the pure absorber problem, however, the pure absorber is replaced by a material which has a scattering cross section of 50% of the total cross section intended as the case where ray effects are not too large. Preliminary results were presented at the Madrid conference by Kobayashi et al. (1999).

2 BENCHMARK PROBLEMS

The systems consist of three regions, source, void and shield regions, whose geometries are shown in Figs. $1 \sim 8$. An $x-z$ or $y-z$ plane geometry and a sketch of Problem 1 are shown in Figs. 1 and 2, respectively. An $x-y$ or $y-z$ plane geometry and a sketch of Problem 2 are shown in Figs. 3 and 4, respectively. Plane geometries and a sketch of Problem 3 are shown in Figs. $5 \sim 8$, which is called the dog leg void duct problem. Reflective boundary conditions are used at the boundary planes $x = 0$, $y = 0$ and $z = 0$, and vacuum boundary conditions at all outer boundaries for all problems.

The cross sections and source strength S are shown in Table 1. The cross section in a void region is assumed to be not zero but 10^{-4}cm^{-1} so that 3D transport programs based on the second order differential form can be used.

Table 1 One-group cross sections and source strength S

			Problem i	Problem ii
Region	S (n cm^{-3}s^{-1})	Σ_t (cm^{-1})	Σ_s (cm^{-1})	
1	1	0.1	0	0.05
2	0	10^{-4}	0	0.5×10^{-4}
3	0	0.1	0	0.05

In problems 1-i, 2-i and 3-i, the systems consist of a pure absorber, and in problems 1-ii, 2-ii and 3-ii, the systems have a scattering cross section of 50% of the total cross section, namely, $\Sigma_s = 0.5\Sigma_t$. It is expected that the total flux distributions at mesh points shown in Tables $2 \sim 4$ be calculated. These mesh points are chosen so that the programs which give the fluxes at the mesh center can be used. It is expected that mesh width, CPU time, the required memory size, and name of computer used should be given.

2.1 Problem 1

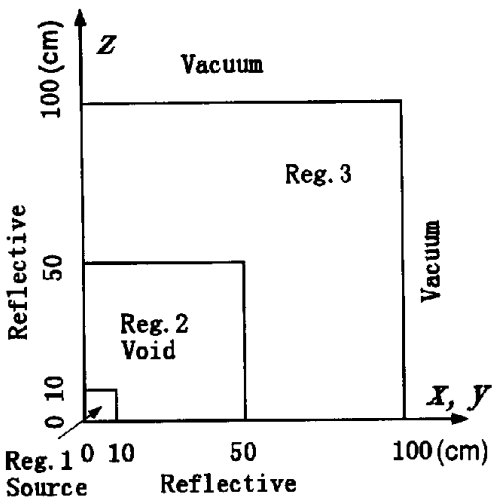

Fig. 1. $x-z$ or $y-z$ plane of Problem 1, Shield with square void

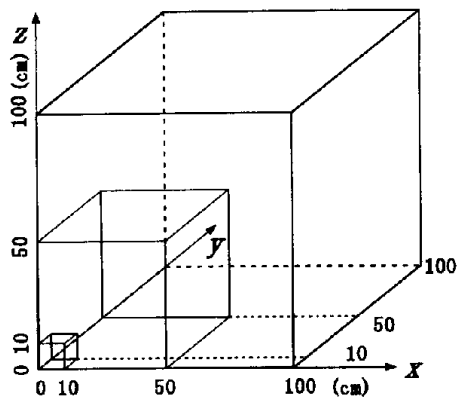

Fig. 2. Sketch of Problem 1, Shield with square void

2.2 Problem 2

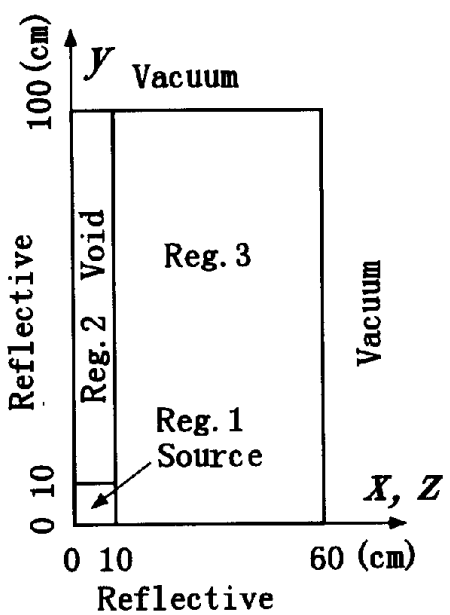

Fig. 3. $x-y$ or $y-z$ plane of Problem 2, Shield with void duct

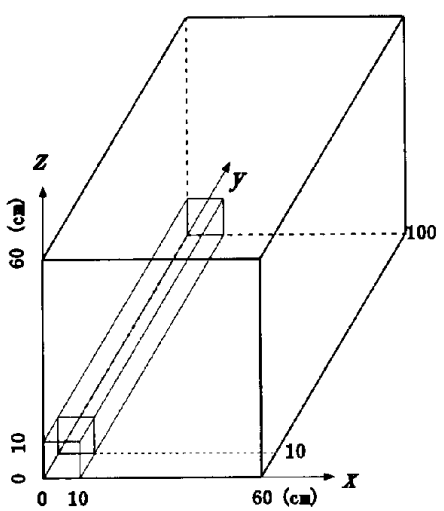

Fig. 4. Sketch of Problem 2, Shield with void duct

2.3 Problem 3

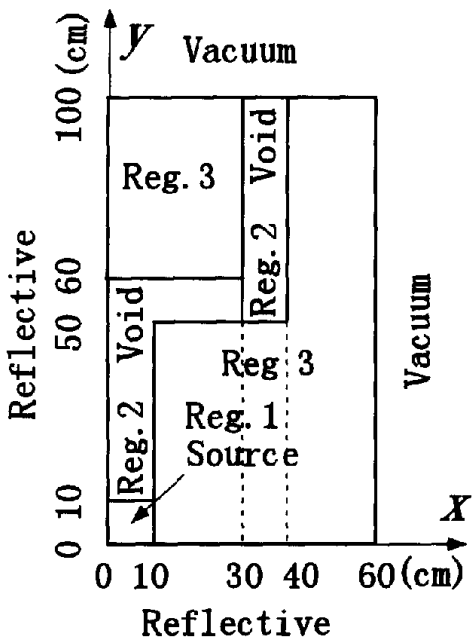

Fig. 5. $x - y$ plane of Problem 3, Shield with dog leg void duct

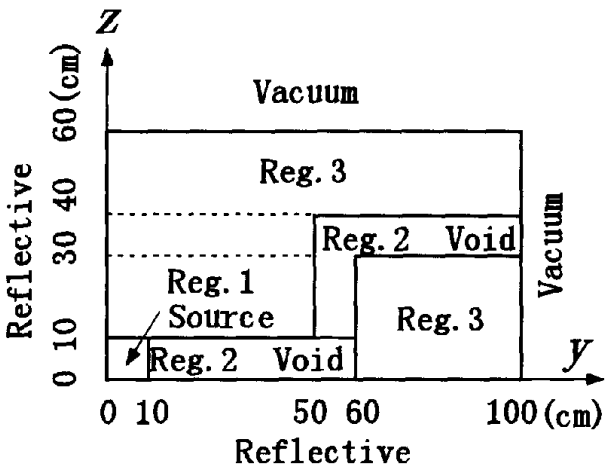

Fig. 6. $y - z$ plane of Problem 3, Shield with dog leg void duct

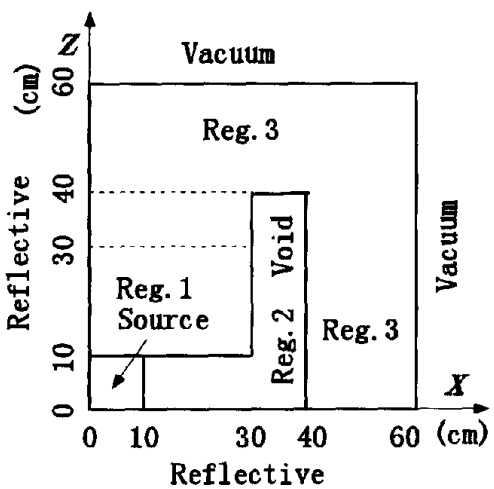

Fig. 7. $x - z$ plane of Problem 3, Shield with dog leg void duct

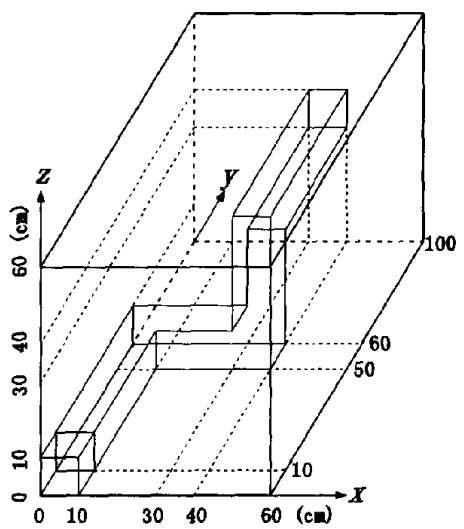

Fig. 8. Sketch of Problem 3, Shield with dog leg void duct

3 REFERENCE SOLUTIONS

3.1 Exact Total Flux for Pure Absorber Problems

In the case of no scattering, fluxes can be obtained simply by numerical integration, namely, the neutron total flux at the observation position $\boldsymbol{r}$ in a pure absorber can be calculated by

$$\phi(\boldsymbol{r}) = \frac{1}{4\pi}\int_{V_s} d\boldsymbol{r}' \frac{\exp(-\int \Sigma_a(\boldsymbol{r}'')d\boldsymbol{r}'')S(\boldsymbol{r}')}{|\boldsymbol{r}-\boldsymbol{r}'|^2}, \tag{1}$$

where $\phi(\boldsymbol{r}), S(\boldsymbol{r}')$, Σ_a and V_s are the total flux, external source, absorption cross section and source region, respectively.

We assume that the source $S(\boldsymbol{r})$ is constant in space and use the relation

$$\boldsymbol{l} = \boldsymbol{r}' - \boldsymbol{r}, \qquad d\boldsymbol{r}' = dl = l^2 dl d\Omega = l^2 dl \sin\theta \, d\varphi \, d\theta, \tag{2}$$

where θ and φ are the polar and azimuthal angles, respectively.

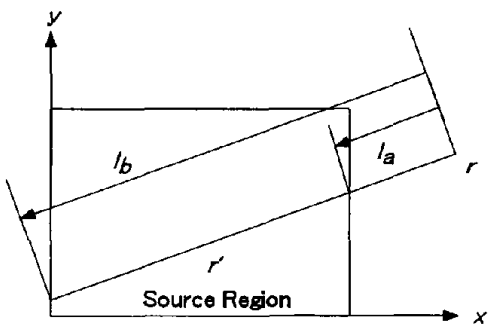

Fig. 9. Observation point is outside the source region

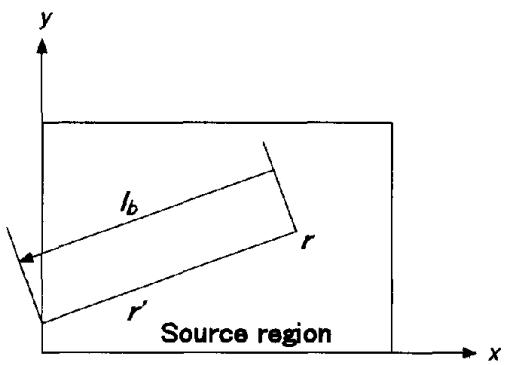

Fig. 10. Observation point is inside the source region

If the observation position $\boldsymbol{r}$ is at the outside of the source region as shown in Fig. 9, the total flux of Eq.(1) can be expressed as

$$\begin{aligned}\phi(\boldsymbol{r}) &= \frac{1}{4\pi}\int_{V_s} d\boldsymbol{l}\frac{\exp(-\int_0^{l_a}\Sigma_a(\boldsymbol{l}')d\boldsymbol{l}' - \int_{l_a}^{l}\Sigma_a(\boldsymbol{l}')d\boldsymbol{l}')S(\boldsymbol{l})}{l^2} \\ &= \frac{S}{4\pi}\int d\Omega\int_{l_a}^{l_b} l^2 dl \frac{\exp(-\Sigma_{a1}l_1 - \Sigma_{a0}l_0)\exp(-\int_{l_a}^{l}\Sigma_{a1}dl')}{l^2} \\ &= \frac{S}{4\pi\Sigma_{a1}}\int d\Omega \exp(-\Sigma_{a1}l_1 - \Sigma_{a0}l_0)(1-\exp(-\Sigma_{a1}(l_b - l_a))),\end{aligned} \tag{3}$$

where the external source is assumed to be in the region whose absorption cross section is Σ_{a1}, l_0 and l_1 are the total length of the path whose absorption cross sections are Σ_{a0} and Σ_{a1}, respectively, and $l_b - l_a$ is the path length in the source region. If the observation position $\boldsymbol{r}$ is in the inside of the source region as shown in Fig. 10, the total flux of Eq.(1) becomes

$$\begin{aligned}\phi(\boldsymbol{r}) &= \frac{1}{4\pi}\int_{V_s} d\boldsymbol{l}\frac{\exp(-\int_0^{l}\Sigma_a(\boldsymbol{l}')d\boldsymbol{l}')S(\boldsymbol{l})}{l^2} = \frac{S}{4\pi}\int d\Omega\int_0^{l_b} l^2 dl\frac{\exp(-\Sigma_{a1}l)}{l^2} \\ &= \frac{S}{4\pi\Sigma_{a1}}\int d\Omega(1-\exp(-\Sigma_{a1}l_b)),\end{aligned} \tag{4}$$

where l_b is the length of the path from the observation position $\boldsymbol{r}$ to the boundary of the source region.

The total fluxes given by Eqs.(3) and (4) are calculated using the trapezoidal rule in θ and φ variables, where the number of mesh points used for both θ and φ variables is 20,000. Convergence with respect to the number of mesh points is checked by comparing the fluxes with 10,000 mesh points and confirming that there is no difference between them. The fluxes thus obtained are shown in Tables 2, 3 and 4 for each problem.

Zmijarevic and Sanchez (2001) also calculated the fluxes from Eq.(1) using three-dimensional numerical quadrature, and their fluxes are exactly the same as the present ones for all six digits given in Tables 2, 3 and 4 except small differences at mesh points (45,95,35) and (55,95,35) of Problem 3.

Table 2 Total flux for Problem 1

Case	Coordinates (cm) (x,y,z)	Case i (No Scattering) Analytical Method Total Flux ($cm^{-2}s^{-1}$)	Case i (No Scattering) Monte Carlo Method by GMVP Total Flux ($cm^{-2}s^{-1}$)	FSD[a] 1σ(%)	Case ii (50% Scattering) Monte Carlo Method by GMVP Total Flux ($cm^{-2}s^{-1}$)	FSD 1σ(%)
1A	5,5,5	5.95659×10^{-0}	5.95332×10^{-0}	0.308	8.29260×10^{-0}	0.021
	5,15,5	1.37185×10^{-0}	1.37116×10^{-0}	0.053	1.87028×10^{-0}	0.005
	5,25,5	5.00871×10^{-1}	5.00789×10^{-1}	0.032	7.13986×10^{-1}	0.003
	5,35,5	2.52429×10^{-1}	2.52407×10^{-1}	0.027	3.84685×10^{-1}	0.004
	5,45,5	1.50260×10^{-1}	1.50251×10^{-1}	0.025	2.53984×10^{-1}	0.006
	5,55,5	5.95286×10^{-2}	5.95254×10^{-2}	0.023	1.37220×10^{-1}	0.073
	5,65,5	1.53283×10^{-2}	1.53274×10^{-2}	0.022	4.65913×10^{-2}	0.117
	5,75,5	4.17689×10^{-3}	4.17666×10^{-3}	0.022	1.58766×10^{-2}	0.197
	5,85,5	1.18533×10^{-3}	1.18527×10^{-3}	0.021	5.47036×10^{-3}	0.343
	5,95,5	3.46846×10^{-4}	3.46829×10^{-4}	0.021	1.85082×10^{-3}	0.619
1B	5,5,5	5.95659×10^{-0}	5.95332×10^{-0}	0.308	8.29260×10^{-0}	0.021
	15,15,15	4.70754×10^{-1}	4.70489×10^{-1}	0.040	6.63233×10^{-1}	0.004
	25,25,25	1.69968×10^{-1}	1.69911×10^{-1}	0.025	2.68828×10^{-1}	0.003
	35,35,35	8.68334×10^{-2}	8.68104×10^{-2}	0.021	1.56683×10^{-1}	0.005
	45,45,45	5.25132×10^{-2}	5.25011×10^{-2}	0.020	1.04405×10^{-1}	0.011
	55,55,55	1.33378×10^{-2}	1.33346×10^{-2}	0.019	3.02145×10^{-2}	0.061
	65,65,65	1.45867×10^{-3}	1.45829×10^{-3}	0.019	4.06555×10^{-3}	0.074
	75,75,75	1.75364×10^{-4}	1.75316×10^{-4}	0.019	5.86124×10^{-4}	0.116
	85,85,85	2.24607×10^{-5}	2.24543×10^{-5}	0.019	8.66059×10^{-5}	0.198
	95,95,95	3.01032×10^{-6}	3.00945×10^{-6}	0.019	1.12982×10^{-5}	0.383
1C	5,55,5	5.95286×10^{-2}	5.95254×10^{-2}	0.023	1.37220×10^{-1}	0.073
	15,55,5	5.50247×10^{-2}	5.50191×10^{-2}	0.023	1.27890×10^{-1}	0.076
	25,55,5	4.80754×10^{-2}	4.80669×10^{-2}	0.022	1.13582×10^{-1}	0.080
	35,55,5	3.96765×10^{-2}	3.96686×10^{-2}	0.021	9.59578×10^{-2}	0.088
	45,55,5	3.16366×10^{-2}	3.16291×10^{-2}	0.021	7.82701×10^{-2}	0.094
	55,55,5	2.35303×10^{-2}	2.35249×10^{-2}	0.020	5.67030×10^{-2}	0.111
	65,55,5	5.83721×10^{-3}	5.83626×10^{-3}	0.020	1.88631×10^{-2}	0.189
	75,55,5	1.56731×10^{-3}	1.56708×10^{-3}	0.020	6.46624×10^{-3}	0.314
	85,55,5	4.53113×10^{-4}	4.53048×10^{-4}	0.020	2.28099×10^{-3}	0.529
	95,55,5	1.37079×10^{-4}	1.37060×10^{-4}	0.020	7.93924×10^{-4}	0.890

a) Fractional standard deviation

Table 3 Total flux for Problem 2

Case	Coordinates (cm) (x,y,z)	Case i (No Scattering) Analytical Method Total Flux ($cm^{-2}s^{-1}$)	Case i (No Scattering) Monte Carlo Method by GMVP Total Flux ($cm^{-2}s^{-1}$)	FSD[a] 1σ(%)	Case ii (50% Scattering) Total Flux ($n\ cm^{-2}s^{-1}$)	FSD 1σ(%)
	5, 5, 5	5.95659×10^{-0}	5.94806×10^{-0}	0.287	8.61696×10^{-0}	0.063
	5, 15, 5	1.37185×10^{-0}	1.37199×10^{-0}	0.055	2.16123×10^{-0}	0.015
	5, 25, 5	5.00871×10^{-1}	5.00853×10^{-1}	0.034	8.93437×10^{-1}	0.011
	5, 35, 5	2.52429×10^{-1}	2.52419×10^{-1}	0.029	4.77452×10^{-1}	0.012
2A	5, 45, 5	1.50260×10^{-1}	1.50256×10^{-1}	0.027	2.88719×10^{-1}	0.013
	5, 55, 5	9.91726×10^{-2}	9.91698×10^{-2}	0.025	1.88959×10^{-1}	0.014
	5, 65, 5	7.01791×10^{-2}	7.01774×10^{-2}	0.024	1.31026×10^{-1}	0.016
	5, 75, 5	5.22062×10^{-2}	5.22050×10^{-2}	0.023	9.49890×10^{-2}	0.017
	5, 85, 5	4.03188×10^{-2}	4.03179×10^{-2}	0.023	7.12403×10^{-2}	0.019
	5, 95, 5	3.20574×10^{-2}	3.20568×10^{-2}	0.022	5.44807×10^{-2}	0.019
	5, 95, 5	3.20574×10^{-2}	3.20568×10^{-2}	0.022	5.44807×10^{-2}	0.019
	15, 95, 5	1.70541×10^{-3}	1.70547×10^{-3}	0.040	6.58233×10^{-3}	0.244
	25, 95, 5	1.40557×10^{-4}	1.40555×10^{-4}	0.046	1.28002×10^{-3}	0.336
2B	35, 95, 5	3.27058×10^{-5}	3.27057×10^{-5}	0.044	4.13414×10^{-4}	0.363
	45, 95, 5	1.08505×10^{-5}	1.08505×10^{-5}	0.042	1.55548×10^{-4}	0.454
	55, 95, 5	4.14132×10^{-6}	4.14131×10^{-6}	0.039	6.02771×10^{-5}	0.599

a) Fractional standard deviation

Table 4 Total flux for Problem 3

Case	Coordinates (cm) (x,y,z)	Case i (No Scattering) Analytical Method Total Flux ($cm^{-2}s^{-1}$)	Case i (No Scattering) Monte Carlo Method by GMVP Total Flux ($cm^{-2}s^{-1}$)	FSD[a] 1σ(%)	Case ii (50% Scattering) Total Flux ($cm^{-2}s^{-1}$)	FSD 1σ(%)
	5, 5, 5	5.95659×10^{-0}	5.93798×10^{-0}	0.306	8.61578×10^{-0}	0.044
	5, 15, 5	1.37185×10^{-0}	1.37272×10^{-0}	0.052	2.16130×10^{-0}	0.010
	5, 25, 5	5.00871×10^{-1}	5.01097×10^{-1}	0.032	8.93784×10^{-1}	0.008
	5, 35, 5	2.52429×10^{-1}	2.52517×10^{-1}	0.027	4.78052×10^{-1}	0.008
	5, 45, 5	1.50260×10^{-1}	1.50305×10^{-1}	0.025	2.89424×10^{-1}	0.009
3A	5, 55, 5	9.91726×10^{-2}	9.91991×10^{-2}	0.024	1.92698×10^{-1}	0.010
	5, 65, 5	4.22623×10^{-2}	4.22728×10^{-2}	0.023	1.04982×10^{-1}	0.077
	5, 75, 5	1.14703×10^{-2}	1.14730×10^{-2}	0.022	3.37544×10^{-2}	0.107
	5, 85, 5	3.24662×10^{-3}	3.24736×10^{-3}	0.021	1.08158×10^{-2}	0.163
	5, 95, 5	9.48324×10^{-4}	9.48534×10^{-4}	0.021	3.39632×10^{-3}	0.275
	5, 55, 5	9.91726×10^{-2}	9.91991×10^{-2}	0.024	1.92698×10^{-1}	0.010
	15, 55, 5	2.45041×10^{-2}	2.45184×10^{-2}	0.035	6.72147×10^{-2}	0.019
	25, 55, 5	4.54477×10^{-3}	4.54737×10^{-3}	0.037	2.21799×10^{-2}	0.028
3B	35, 55, 5	1.42960×10^{-3}	1.43035×10^{-3}	0.034	9.90646×10^{-3}	0.033
	45, 55, 5	2.64846×10^{-4}	2.64959×10^{-4}	0.032	3.39066×10^{-3}	0.195
	55, 55, 5	9.14210×10^{-5}	9.14525×10^{-5}	0.029	1.05629×10^{-3}	0.327
	5, 95, 35	3.27058×10^{-5}	3.27087×10^{-5}	0.045	3.44804×10^{-4}	0.793
	15, 95, 35	2.68415×10^{-5}	2.68518×10^{-5}	0.047	2.91825×10^{-4}	0.659
	25, 95, 35	1.70019×10^{-5}	1.70104×10^{-5}	0.047	2.05793×10^{-4}	0.529
3C	35, 95, 35	3.37981×10^{-5}	3.38219×10^{-5}	0.043	2.62086×10^{-4}	0.075
	45, 95, 35	6.04893×10^{-6}	6.05329×10^{-6}	0.042	1.05367×10^{-4}	0.402
	55, 95, 35	3.36460×10^{-6}	3.36587×10^{-6}	0.028	4.44962×10^{-5}	0.440

a) Fractional standard deviation

3.2 Monte Carlo Results by GMVP

Monte Carlo calculations were also performed using GMVP (Mori and Nakagawa, 1994), where a point-detector estimator was used to tally the total flux at the given calculation points for all cases. In the pure absorber cases, 10^7 histories were used, and for the 50% scattering cases, 10^9, 10^8 and 2×10^8 histories for Problems 1, 2 and 3, respectively. Calculated total fluxes are shown in Tables $2 \sim 4$. The total fluxes for the pure absorber cases are in very good agreement with the analytical results, which shows that the program GMVP is reliable for this kind of problems. Konno (2001) also calculated the total flux using MCNP4B2, and his results agree well with the present results within statistical errors.

4 BENCHMARK RESULTS

As shown in Table 5, there are eight contributions for the present benchmarks. Six contributions were obtained by using discrete ordinates method programs. They are: TORT by Azmy et al. (2001) at ORNL, TORT with FNSUNCL3 (Kosako and Konno,1998) by Konno (2001) at JAERI, PARTISN by Alcouffe (2001) at LANL, PENTRAN by Haghighat and Sjoden (2001) at PSU and USAF respectively, IDT by Zmijarevic and Sanchez (2001), and MCCG3D by Suslov (2001) at CEA. The other two contributions were obtained using the spherical harmonics method, EVENT by Oliveira et al. (2001) at IC, and ARDRA by Brown et al. (2001) at LLNL.

In the results by Konno, there are two cases, one in which only TORT is used, and the other in which TORT is used together with the program FNSUNCL3 and for which the first flight collision source is calculated. In the finite element-spherical harmonics solutions by EVENT, the ray-tracing method has been used in the void region, and the flux values are quoted only for points within the domain of the non-void region, since fluxes in the ray-tracing regions were not available with the current implementation.

Table 5 3D Transport Benchmark Results

Name	Program	Method	Problems	Mesh Width (cm)	Computer
Azmy, et al.	TORT	S_{16} LN[a]	scattering cases only	10/9	Cray Y/MP 4 tasks
Konno	TORT	S_{16}	all cases	2	FUJITSU
	TORT with FNSUNCL3	S_{16} FCS[b]	all cases	2 0.25	AP3000/24
Alcouffe	PARTISN	S_8, FC[b]	all cases	2	SGI
Haghighat, et al.	PENTRAN	S_{20}, ADS[c]	no scattering	Variable(2 – 10)	IBM SP2
		S_{12}, ADS[c]	scattering	1.111	IBM SP2
Zmijarevic, et al.	IDT	S_{16}, LC[d] Extrapolated	all cases	(10/9)	DEC Alpha 4100
Suslov	MCCG3D	RT[e], SC[f], DD[g]	all cases	2.5	SP2
Oliveira, et al.	EVENT	P_9, RT[e]	all cases	1.43 – 2	COMPAQ AXP 1000
Brown, et al.	ARDRA	P_{21}	all cases	1.04-2	IBM ASCI Blue-Pacific

a) Linear Nodal b) First Collision Source
c) Adaptive Differencing Strategy using the DTW and EDW schemes d) Linear Characteristic
e) Ray Tracing f) Step Characteristic g) Diamond Difference

Benchmark results for Problem (i) of no scattering and (ii) of 50% scattering for three Problems 1,2 and 3 are shown in Figs. 11 $\sim$ 42. Shown in these Figures are the scattering cases calculated with TORT by Azmy, and the no-scattering cases calculated with TORT by Konno. In Figs. 12, 14, etc., the ratios of the fluxes to the reference values (i.e. the exact values by the analytical method for the pure absorber cases, and the Monte Carlo values for the scattering cases) are shown in order to make clear the difference from the reference values.

5 DISCUSSION AND CONCLUSION

The benchmark results shown in Figs. 11 $\sim$ 42 are fairly close to the reference solutions, although some preliminary results have some discrepancies with regard to the reference solutions. In the case of the pure absorber, the apparent discrepancies of the discrete ordinates program TORT(JAERI) from the exact values for problems 1Ci, 2Bi and 3Ci may be due to the ray effect. Namely, even the S_{16} method gives appreciable errors due to ray effects.

In the cases with 50% scattering, the total fluxes for the problems, for example, 1Cii, 2Bii and 3Cii are larger by about a factor 10 than those for pure absorber cases of 1Ci, 2Bi and 3Ci, respectively. Namely, the number of scattered neutrons is larger by about a factor 10 than the neutrons which come directly from the source, and the ray effect becomes smaller even in TORT. However, discrepancies from the exact values are fairly large for the problem of the dog leg duct, problems 3Ci and 3Cii. In the discrete ordinates programs TORT, PENTRAN and IDT, the first collision source was not used. In PENTRAN, the ray effect is remedied by using appropriate angular and spatial meshes and mesh widths, and PENTRAN's unique differencing formulations including adaptive differencing strategy with directional theta-weighted (DTW) and exponential directional weighted (EDW) schemes and Taylor projection mesh coupling (TPMC)(Haghighat and Sjoden, 2001).

In other discrete ordinates programs, TORT with FNSUNCL3, PARTISN and MCCG3D, the first collision source was used to remedy the ray effect, which is seen in figures given by Konno (2001) to be very successful. Namely, the use of the first collision source for the discrete ordinates method improved the accuracy appreciably for both problems of pure absorber and 50% scattering cases. In particular, the results of MCCG3D and TORT with FNSUNCL3 are in excellent agreement, within an error of 1% $\sim$5% with the reference solution in most cases and can be considered as an independent confirmation of the reference solution. It should be noted that, for the pure absorber problems, the first collision source method should give in principle exact fluxes and this fact does not demonstrate the accuracy of the discrete ordinate method itself.

An advantage of the spherical harmonics method is that the equations are invariant under rotation of the coordinates and do not depend on the direction of the coordinates, that should give no ray effect. In order to overcome the difficulty in deriving the discretized equations of the spherical harmonics method for void problems, the ray-tracing method was used for the void region in the spherical harmonics program EVENT, and the flux in non-void region was coupled with the current in the void region at the void-material interface. Using this method, the accuracy of the current spherical harmonics method program was improved. In the program ARDRA, the discrete ordinates equations with a fictitious source were solved in such a way that the equations became equivalent to those of the spherical harmonics method, which were used to solve two dimensional spherical harmonics equations (Reed, 1972, Jung et al. 1974).

As seen in the figures, the accuracy of the discrete ordinates method with the first collision source is best for the present benchmark problems. It is expected that the present benchmark problem would help further improvement of 3D transport programs based on the spherical harmonics method as well as the discrete ordinates method.

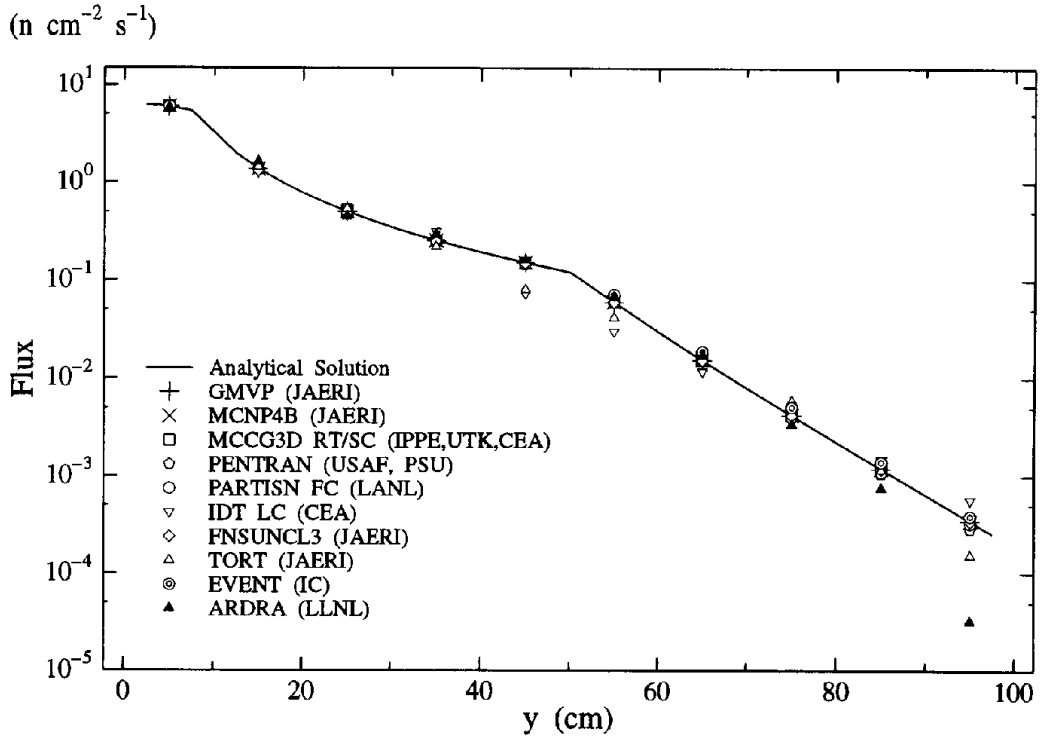

Fig. 11. Problem 1Ai "No scattering" ($x = z = 5$ cm)

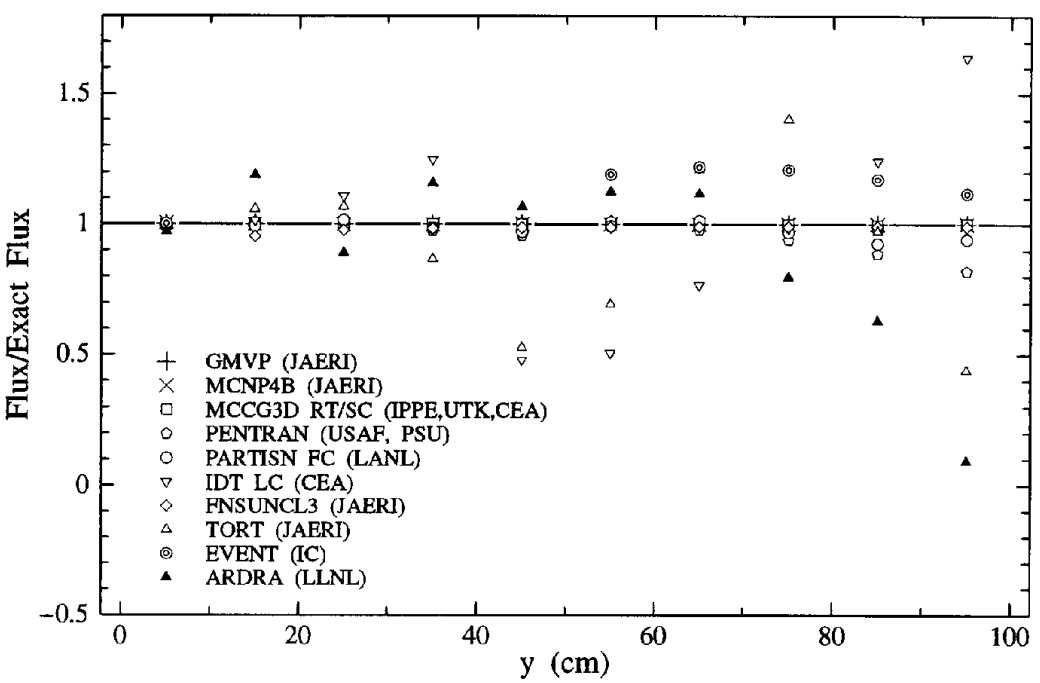

Fig. 12. Relative flux of problem 1Ai ($x = z = 5$ cm)

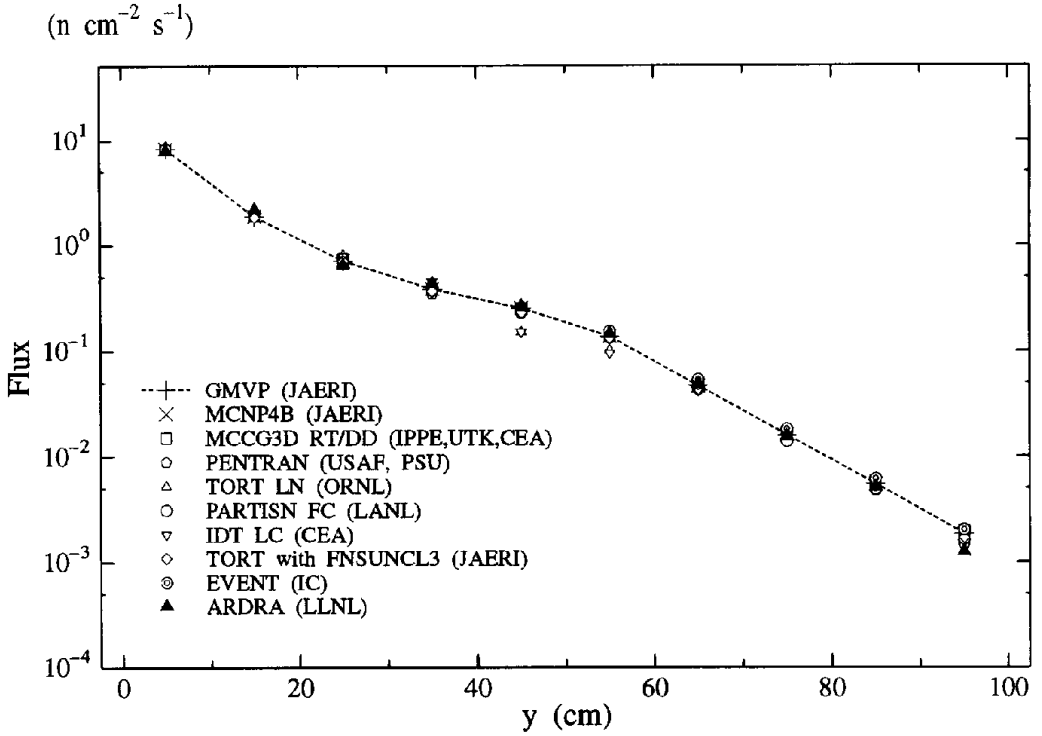

Fig. 13. Problem 1Aii "50% scattering" ($x = z = 5$ cm)

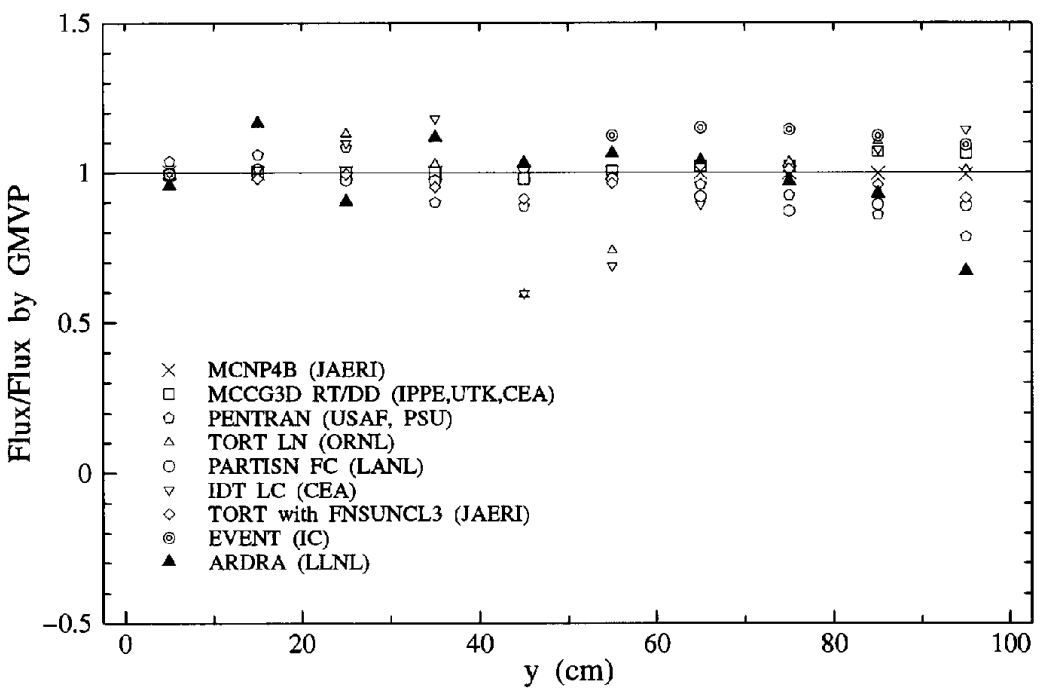

Fig. 14. Relative flux of problem 1Aii ($x = z = 5$ cm)

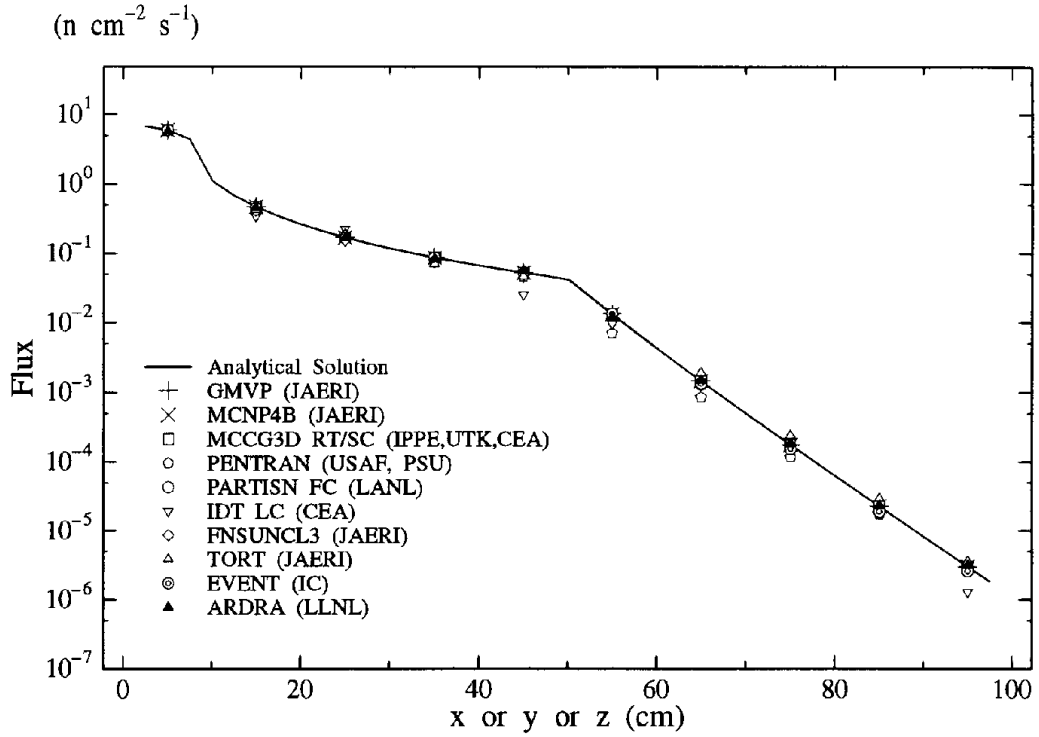

Fig. 15. Problem 1Bi "No scattering" ($x = y = z$)

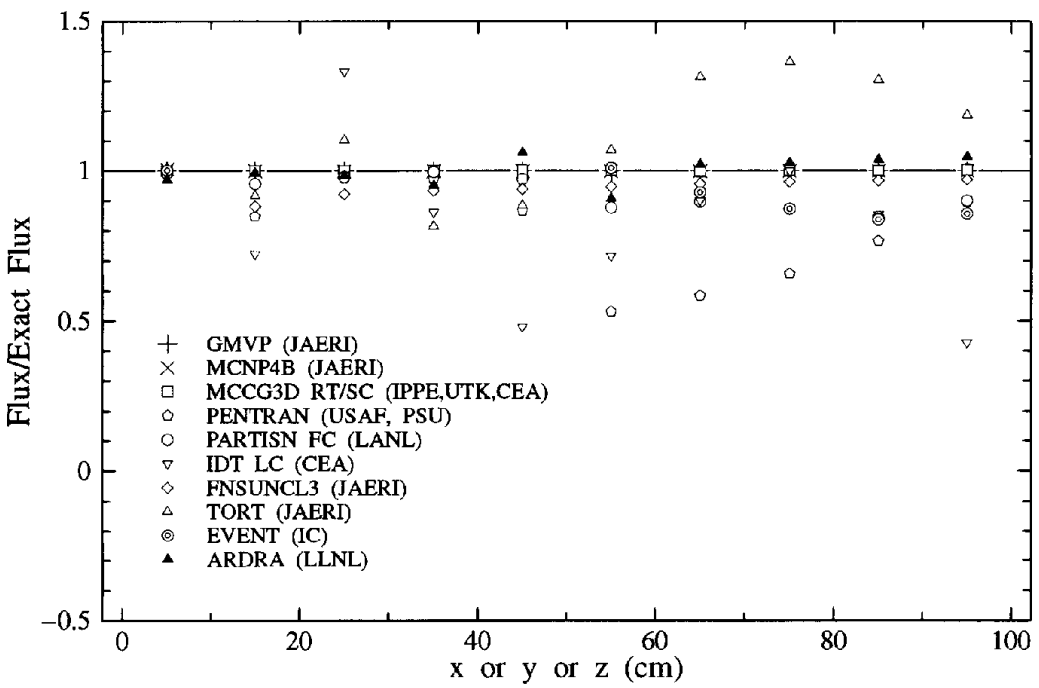

Fig. 16. Relative flux of problem 1Bi ($x = y = z$)

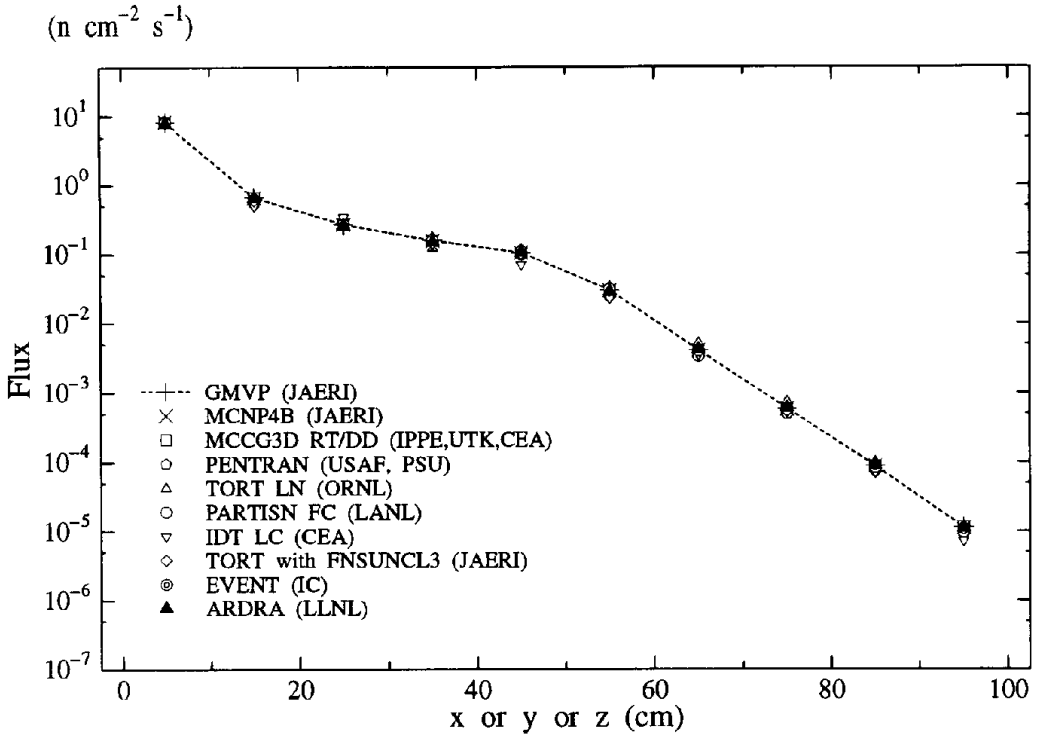

Fig. 17. Problem 1Bii "50% scattering" $(x = y = z)$

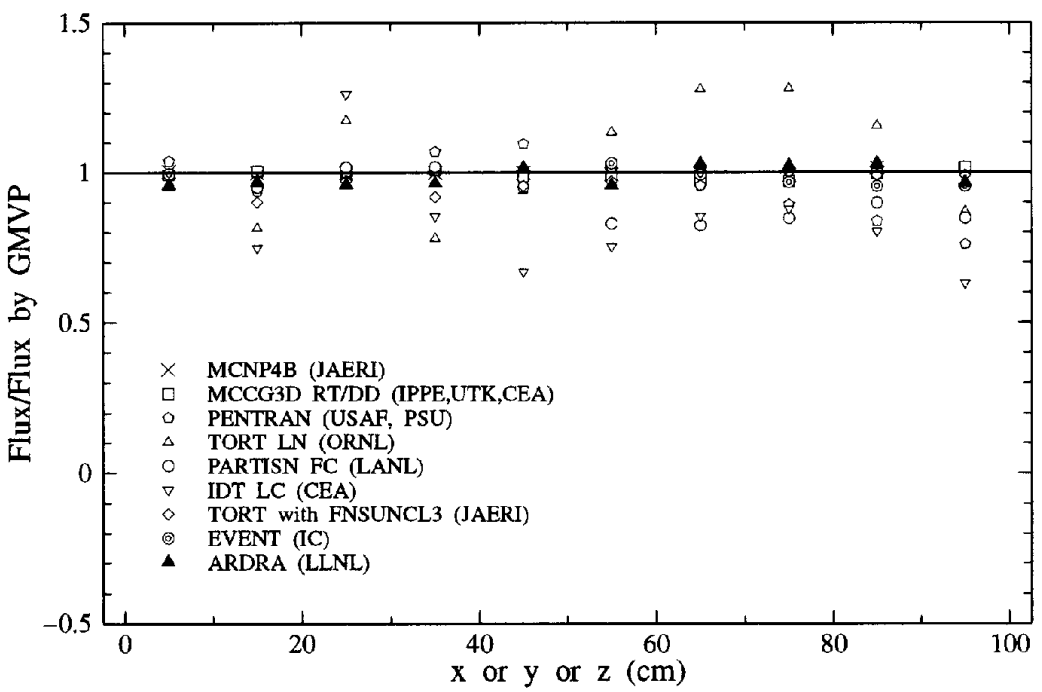

Fig. 18. Relative flux of problem 1Bii $(x = y = z)$

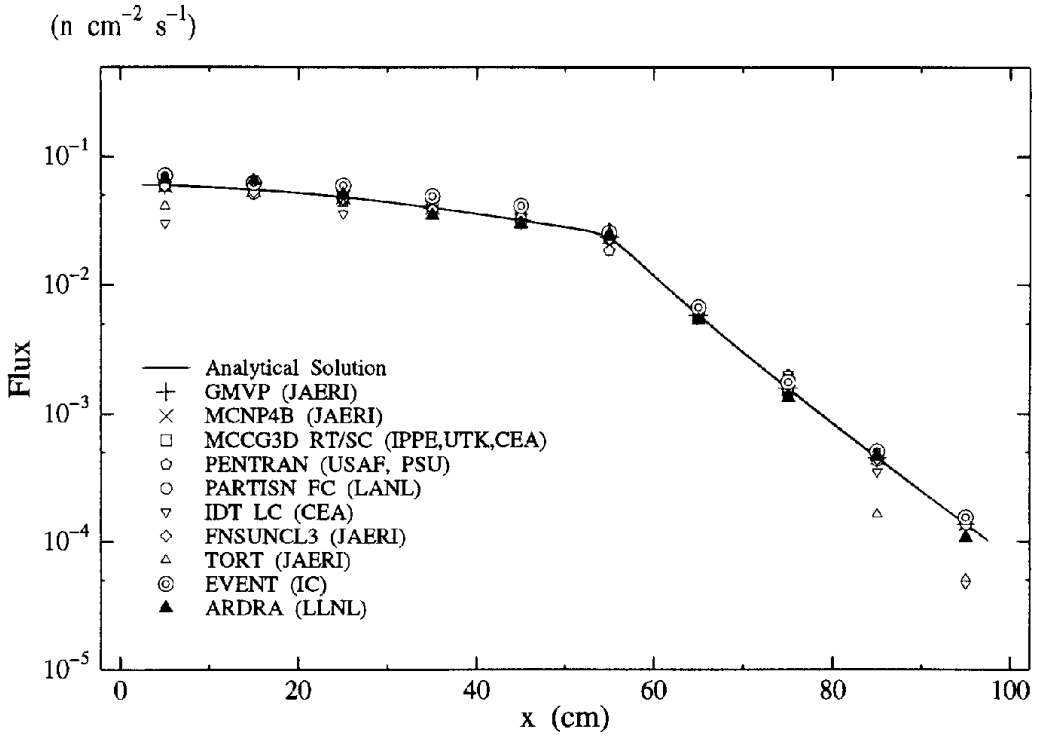

Fig. 19. Problem 1Ci "No scattering" ($y = 55$ cm, $z = 5$ cm)

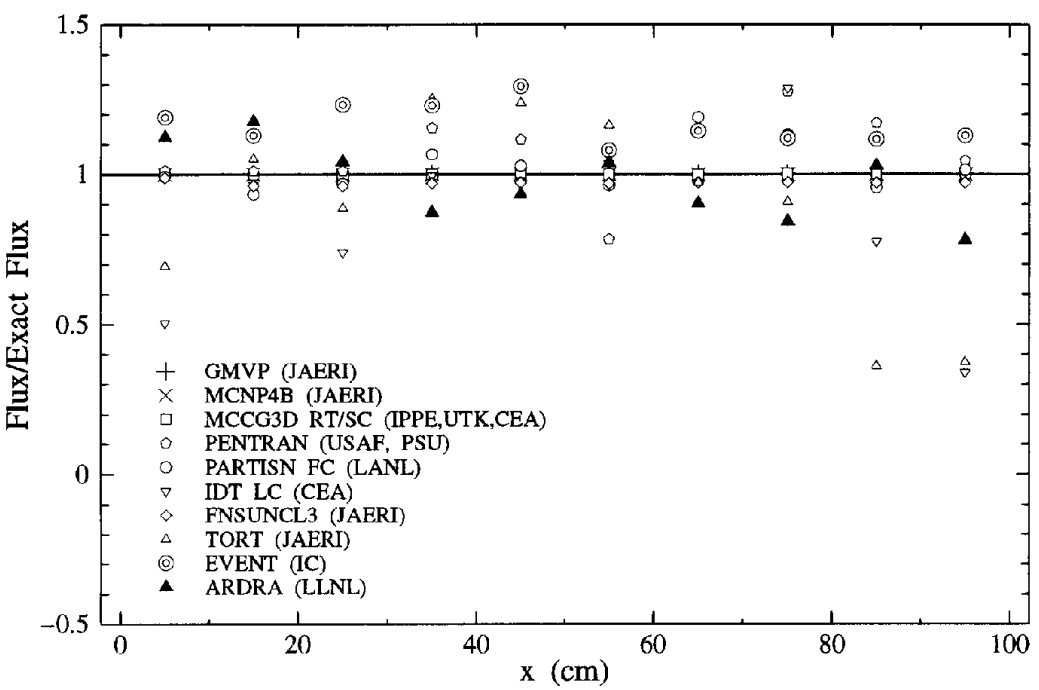

Fig. 20. Relative flux of problem 1Ci ($y = 55$ cm, $z = 5$ cm)

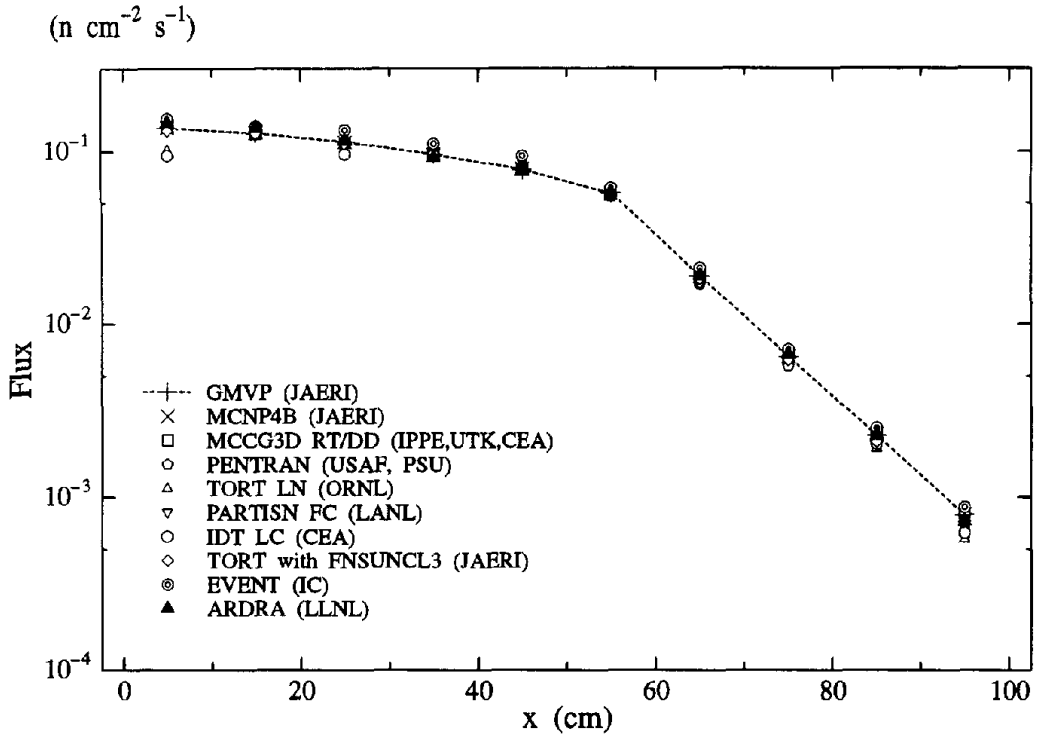

Fig. 21. Problem 1Cii "50% scattering" ($y = 55$ cm, $z = 5$ cm)

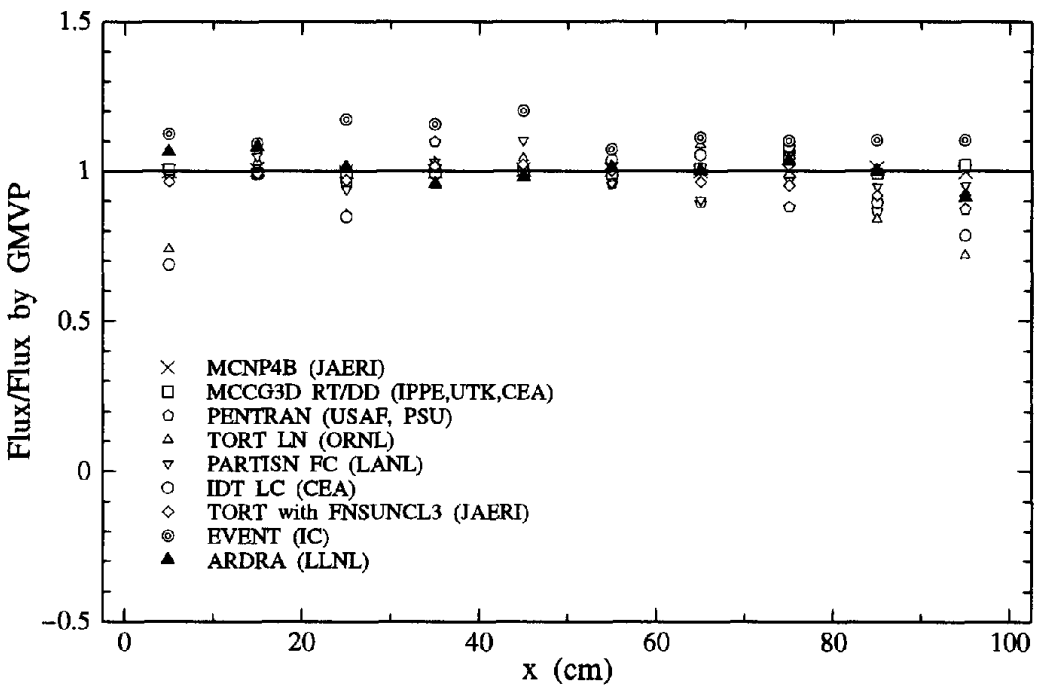

Fig. 22. Relative flux of problem 1Cii ($y = 55$ cm, $z = 5$ cm)

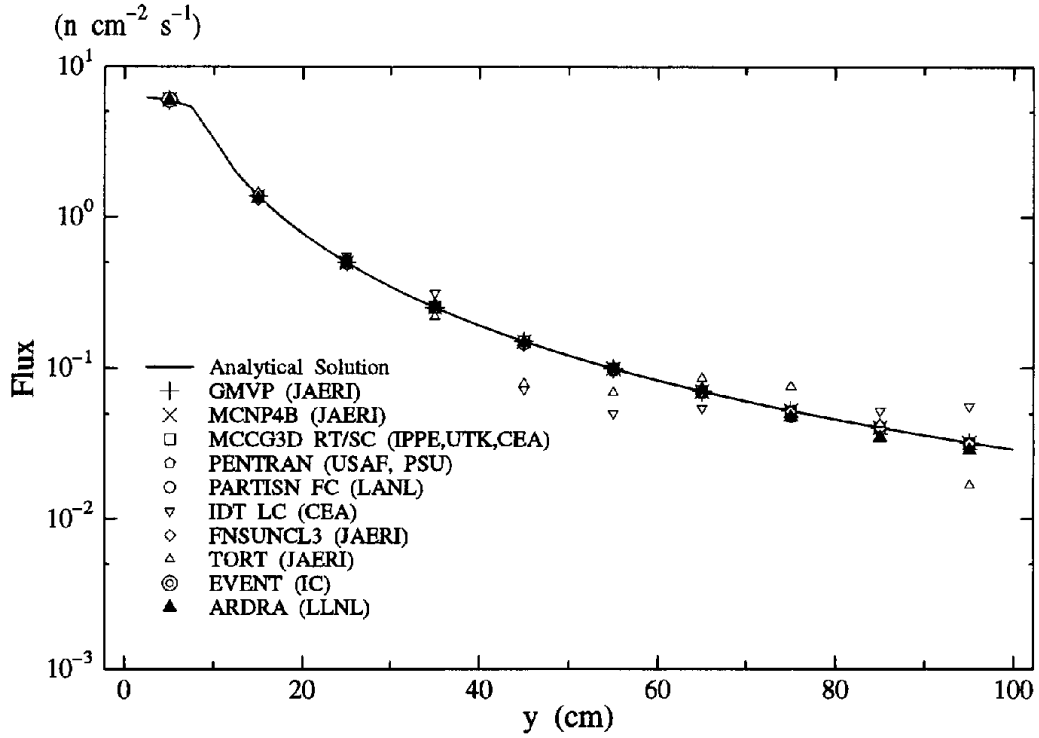

Fig. 23. Problem 2Ai "No scattering" ($x = z = 5$ cm)

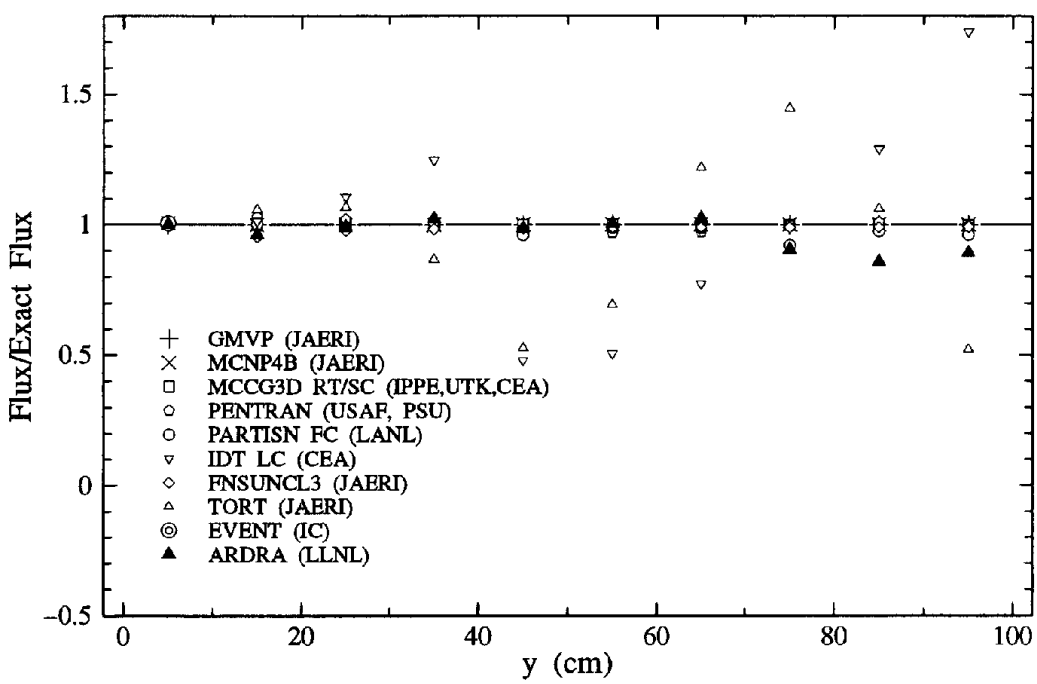

Fig. 24. Relative flux of problem 2Ai ($x = z = 5$ cm)

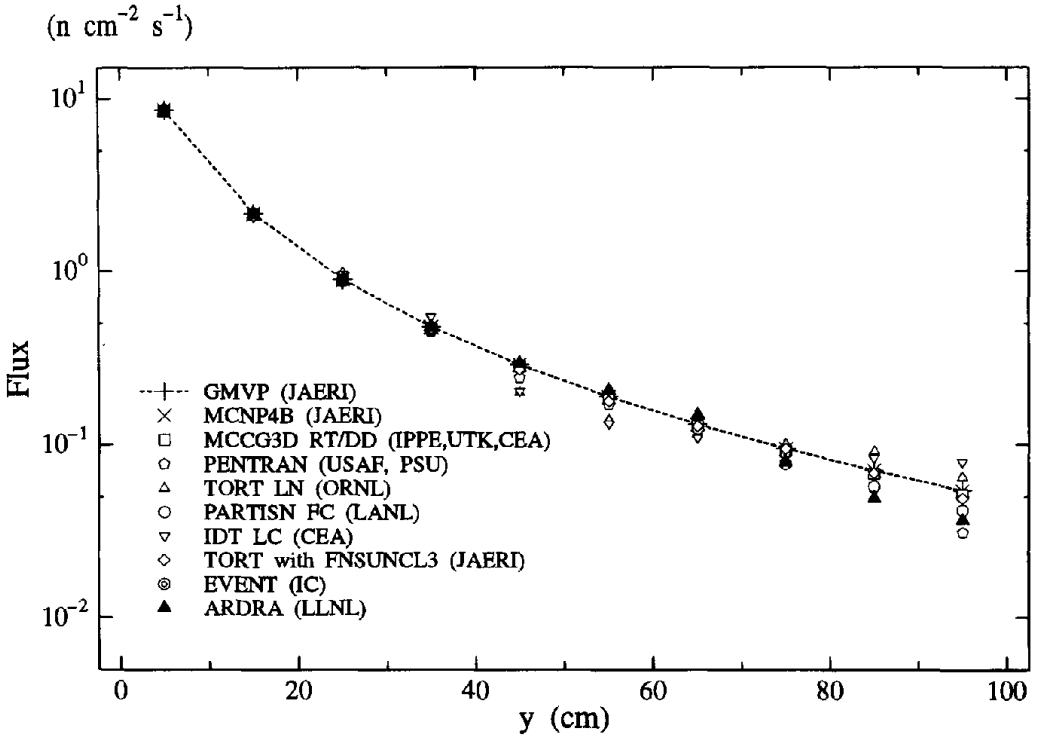

Fig. 25. Problem 2Aii "50% scattering" ($x = z = 5$ cm)

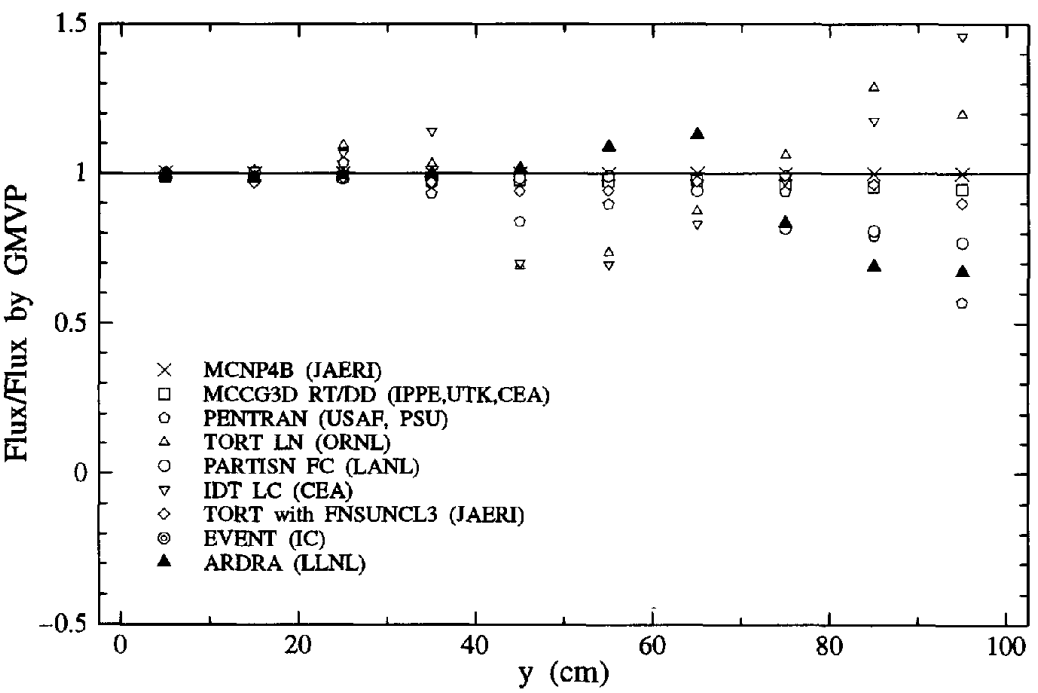

Fig. 26. Relative flux of problem 2Aii ($x = z = 5$ cm)

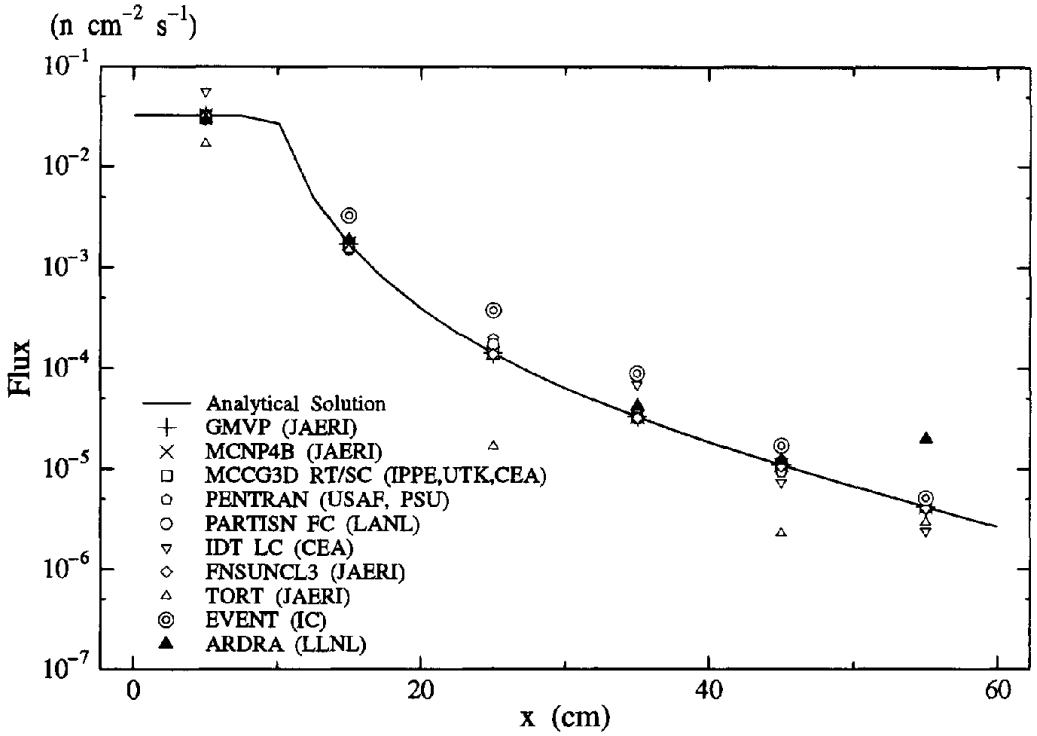

Fig. 27. Problem 2Bi "No scattering" ($y = 95$ cm, $z = 5$ cm)

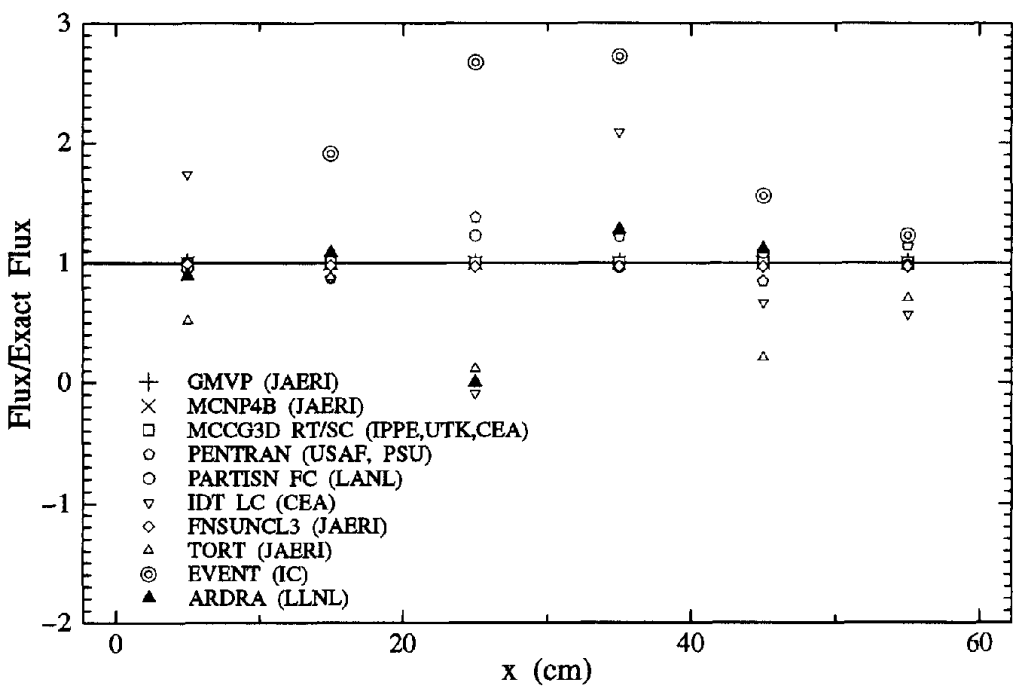

Fig. 28. Relative flux of problem 2Bi ($y = 95$ cm, $z = 5$ cm)

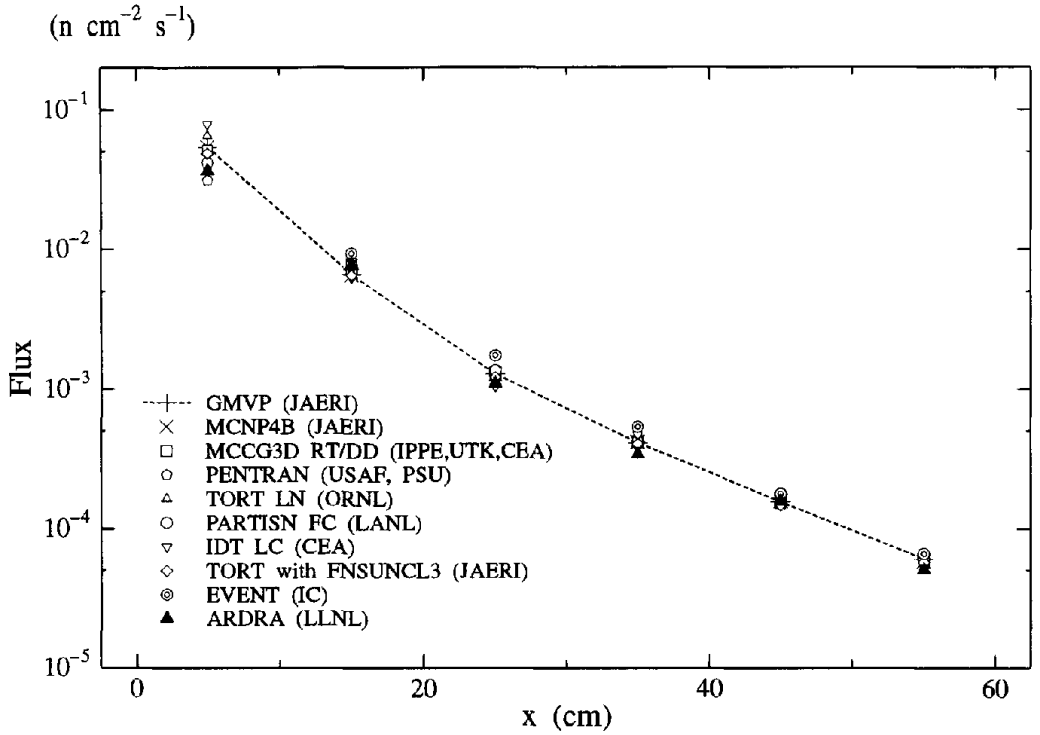

Fig. 29. Problem 2Bii "50% scattering" ($y = 95$ cm, $z = 5$ cm)

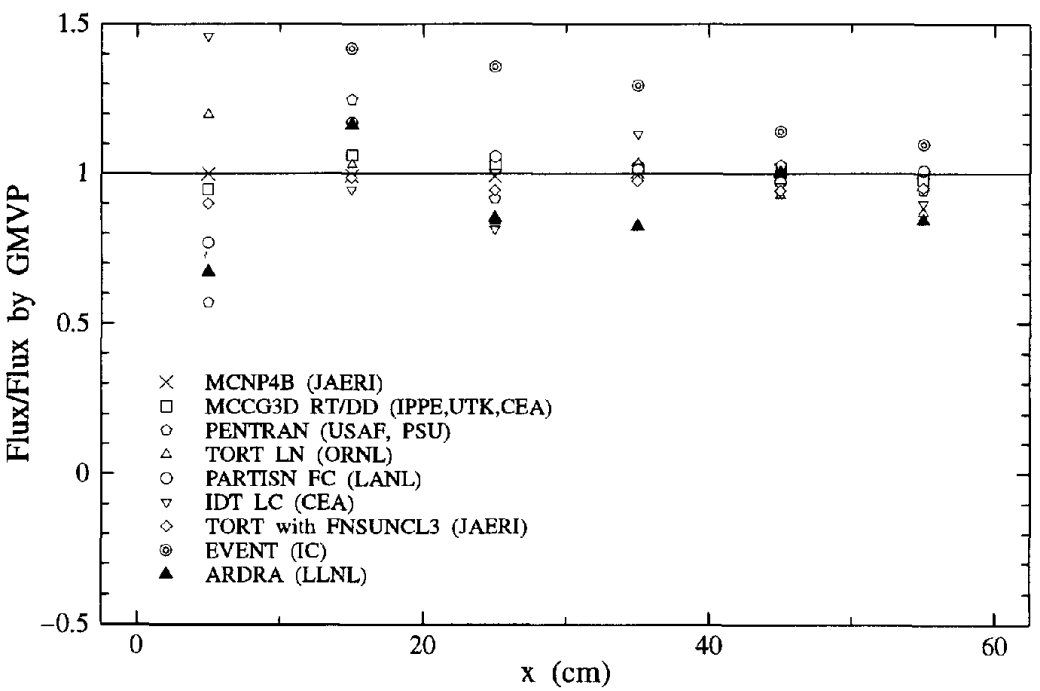

Fig. 30. Relative flux of problem 2Bii ($y = 95$ cm, $z = 5$ cm)

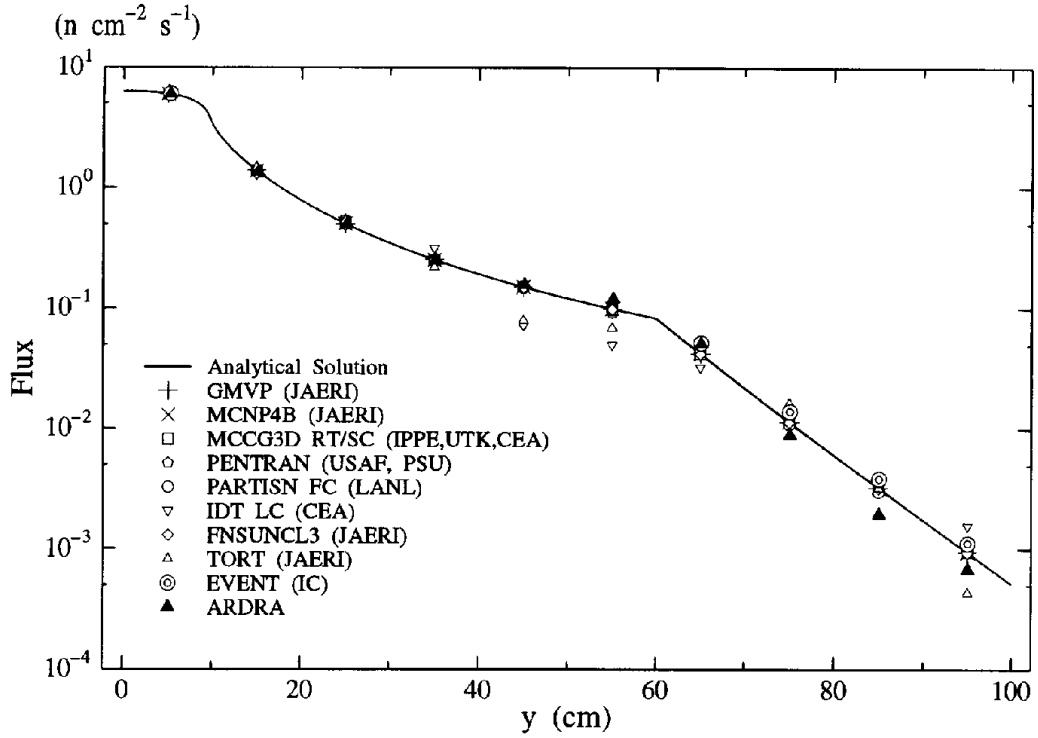

Fig. 31. Problem 3Ai "No scattering" ($x = z = 5$ cm)

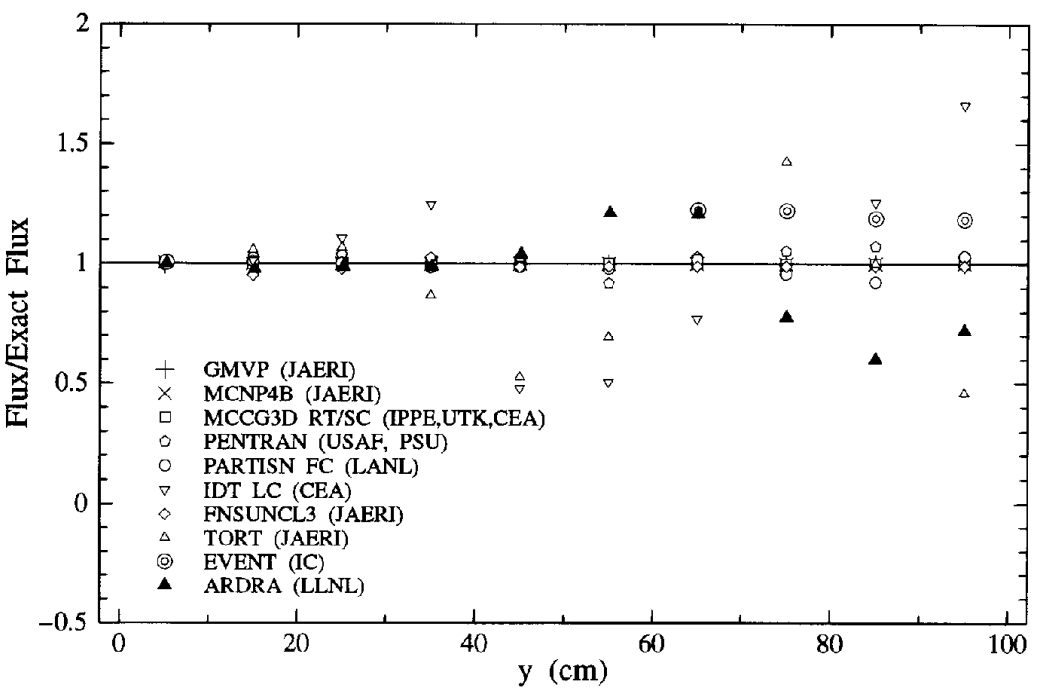

Fig. 32. Relative flux of problem 3Ai ($x = z = 5$ cm)

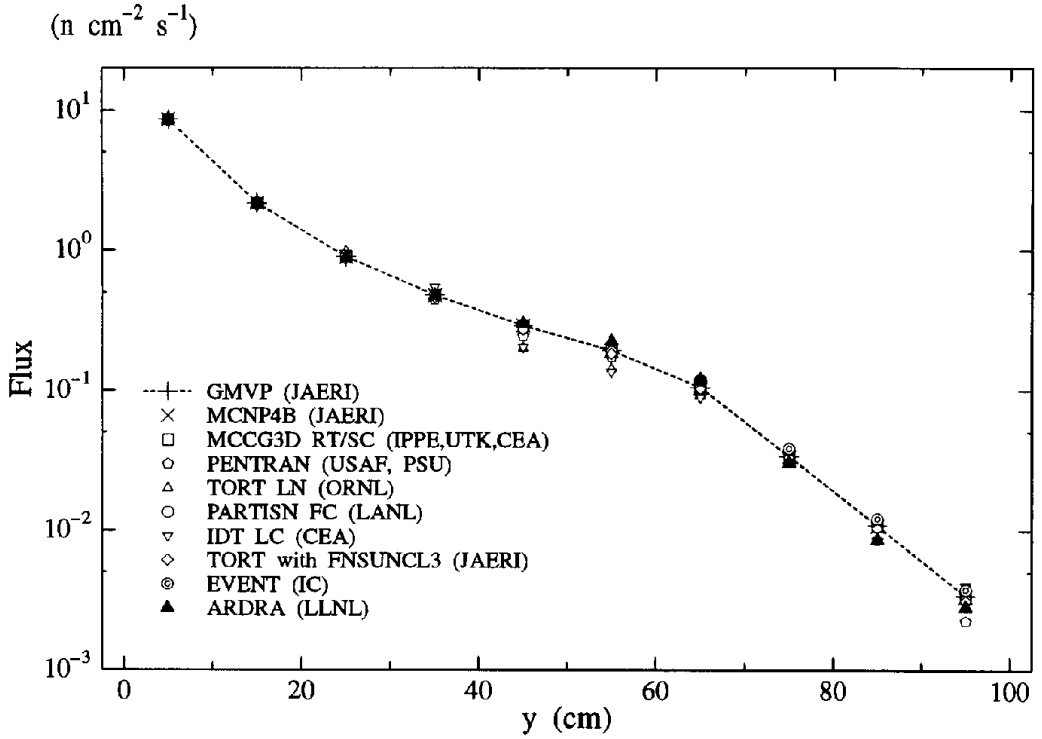

Fig. 33. Problem 3Aii "50% scattering" ($x = z = 5$ cm)

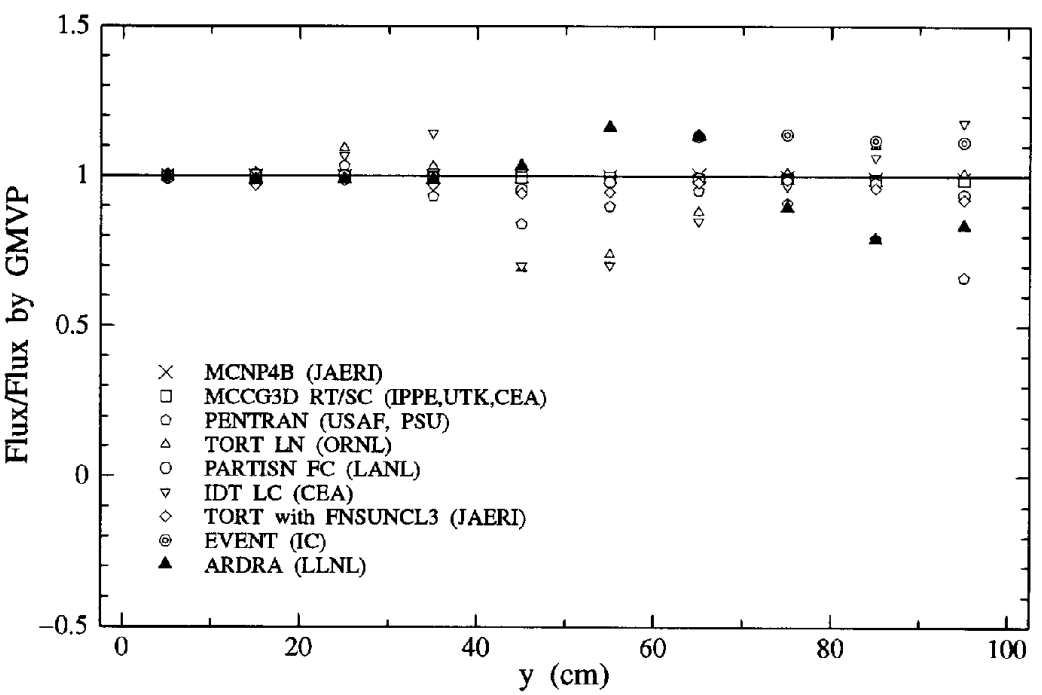

Fig. 34. Relative flux of problem 3Aii ($x = z = 5$ cm)

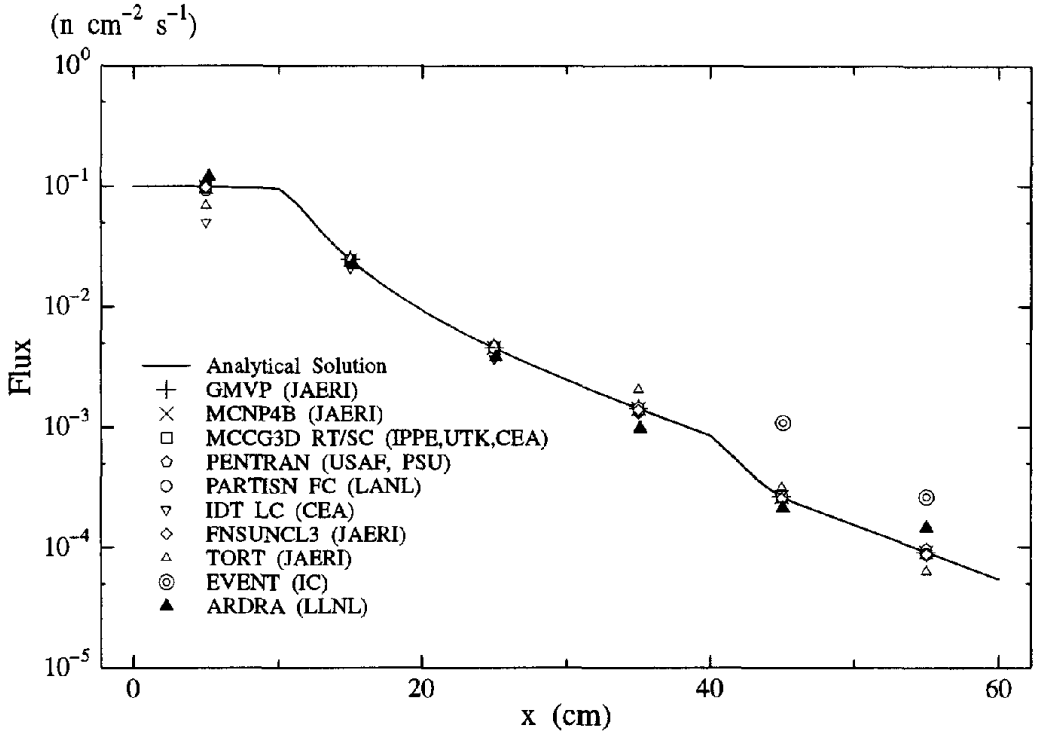

Fig. 35. Problem 3Bi "No scattering" (y = 55 cm, z = 5 cm)

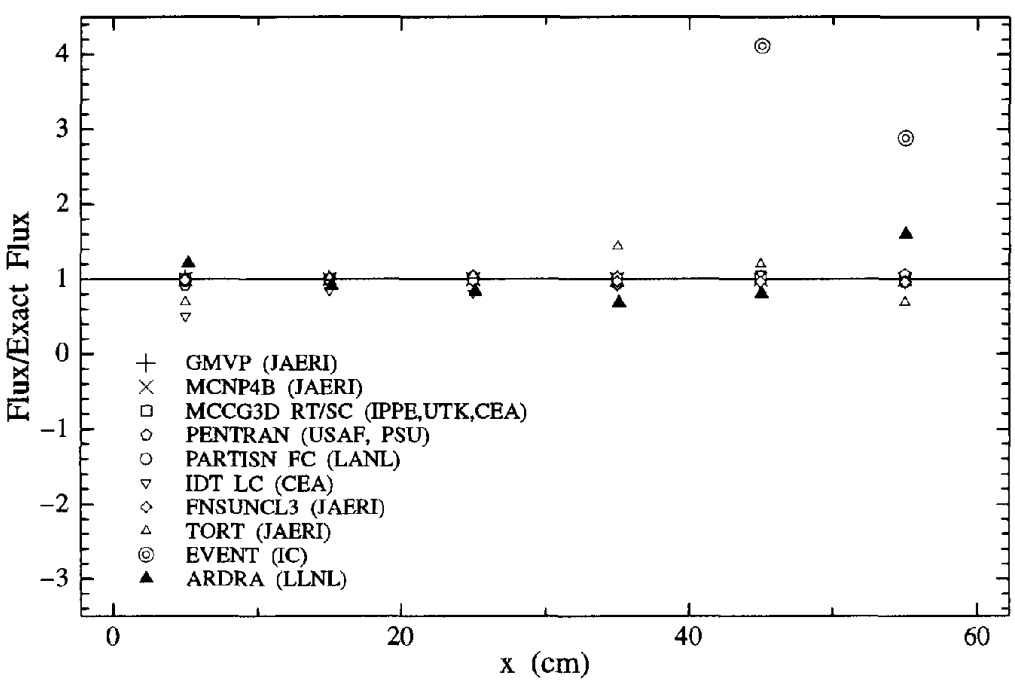

Fig. 36. Relative flux of problem 3Bi (y = 55 cm, z = 5 cm)

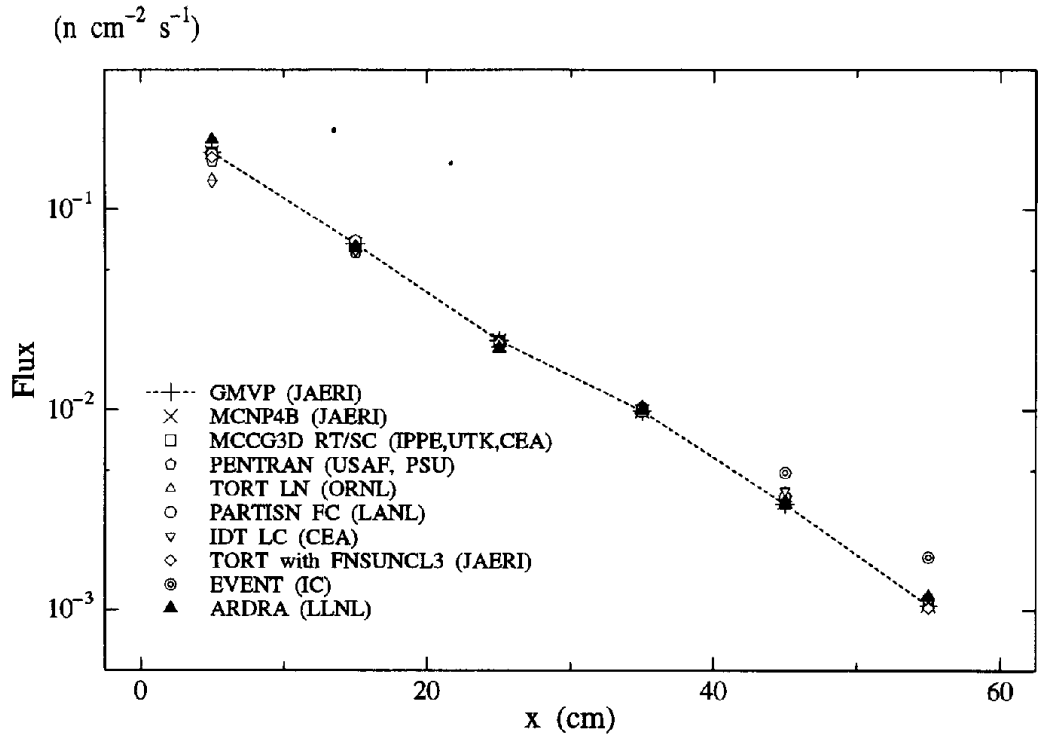

Fig. 37. Problem 3Bii "50% scattering" ($y = 55$ cm, $z = 5$ cm)

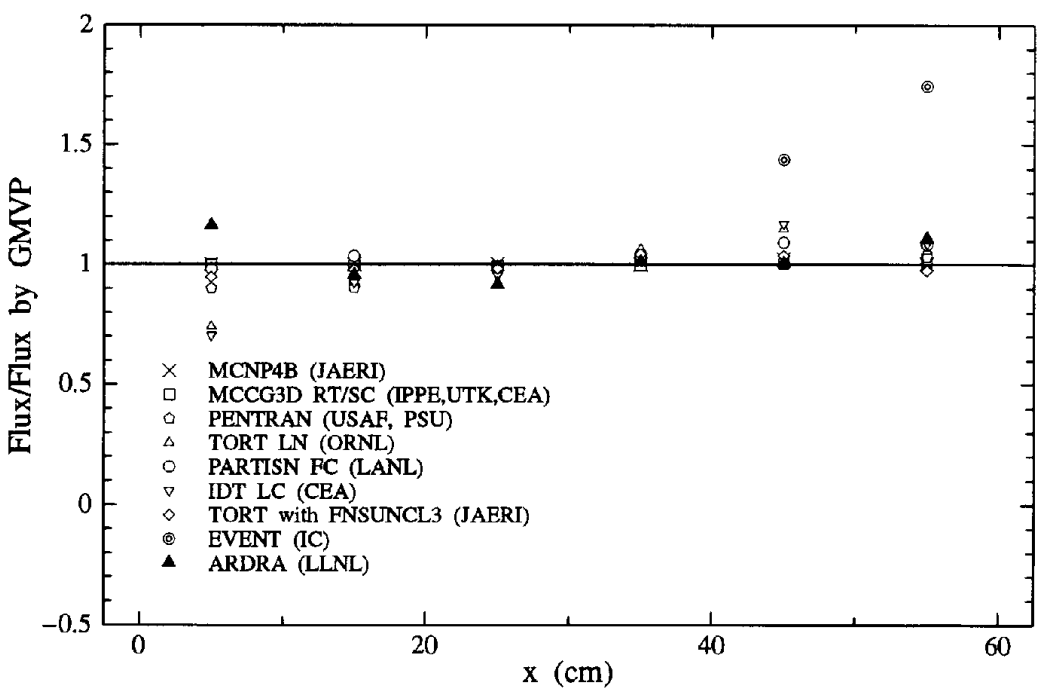

Fig. 38. Relative flux of problem 3Bii ($y = 55$ cm, $z = 5$ cm)

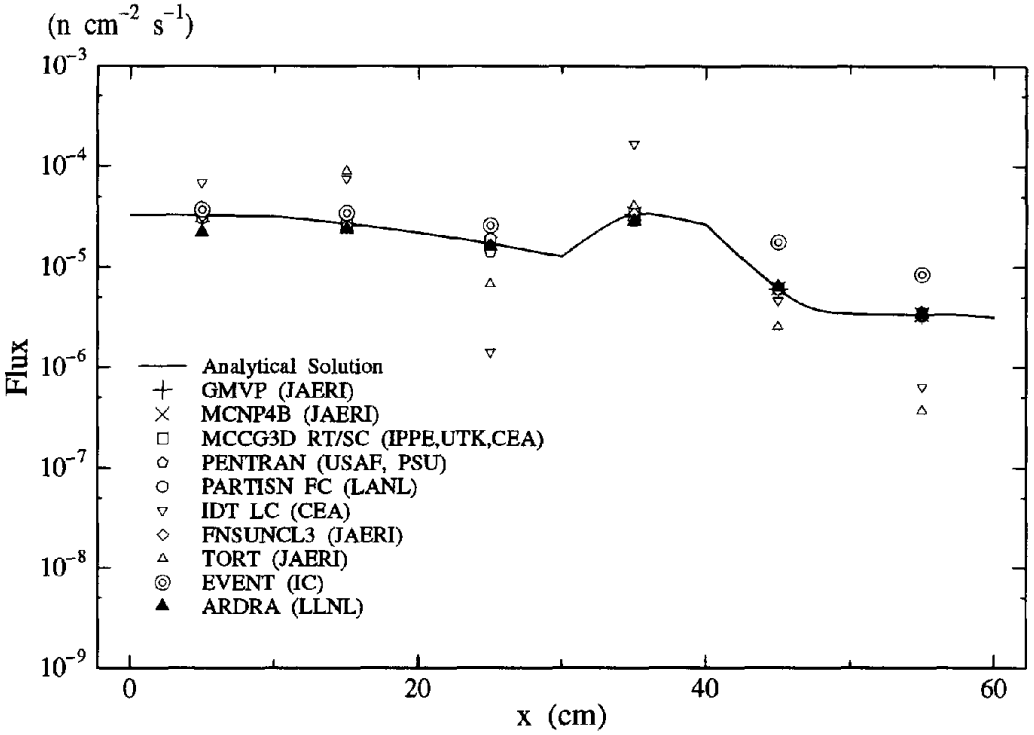

Fig. 39. Problem 3Ci "No scattering" ($y = 95$ cm, $z = 35$ cm)

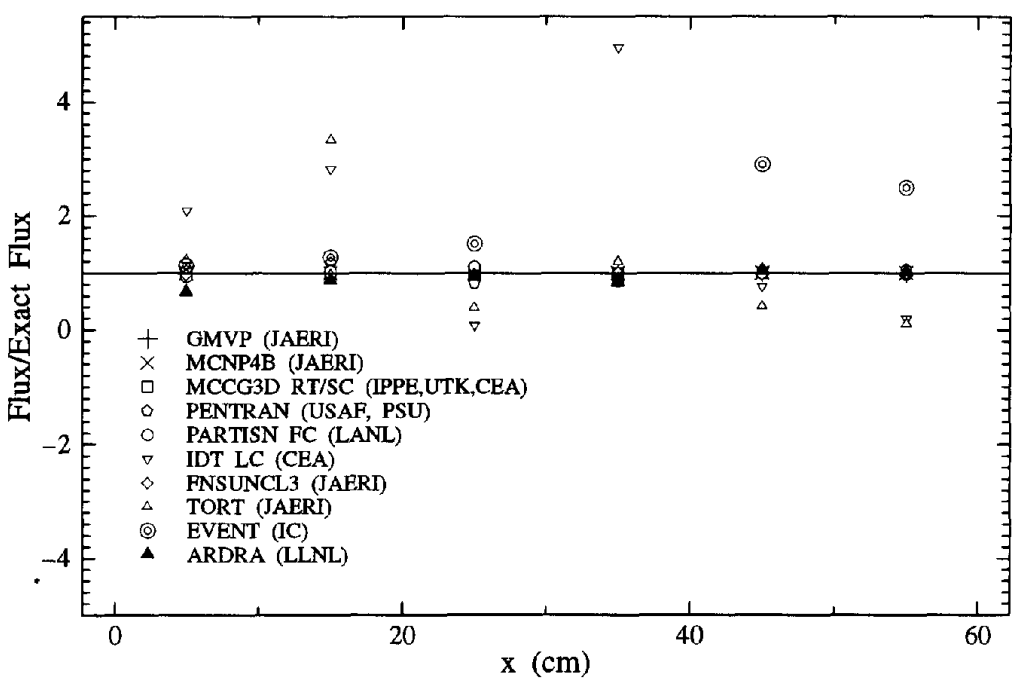

Fig. 40. Relative flux of problem 3Ci ($y = 95$ cm, $z = 35$ cm)

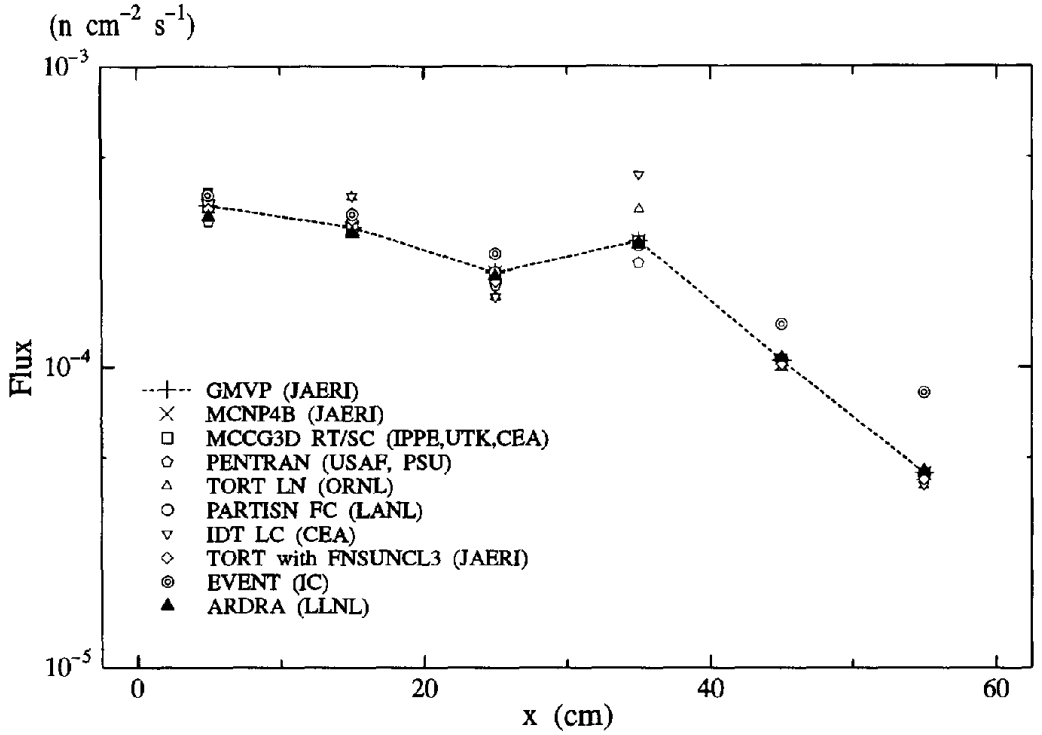

Fig. 41. Problem 3Cii "50% scattering" ($y = 95$ cm, $z = 35$ cm)

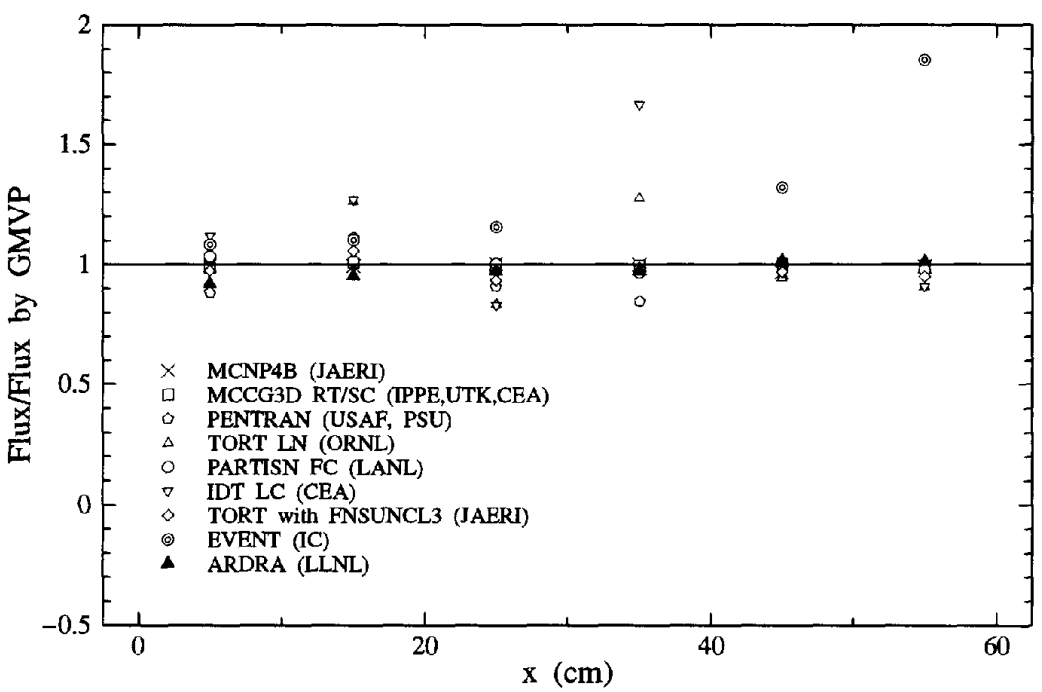

Fig. 42. Relative flux of problem 3Cii ($y = 95$ cm, $z = 35$ cm)

ACKNOWLEDGEMENTS

The authors wish to express their sincere thanks to Richard Sanchez for providing exact values of the pure absorber cases, by which the exact values could be confirmed by the independent method. They would like also to thank the participants for their contribution to this benchmark, E. Sartori of OECD/NEA for his support to this benchmark, and E. Kiefhaber of Forschungszentrum Karlsruhe and Y. Azmy of ORNL for their useful comments to improve the manuscript.

REFERENCES

Ackroyd, R.T. and Riyait, N.S. (1989), Iteration and Extrapolation Method for the Approximate Solution of the Even-Parity Transport Equation for Systems with Voids, *Ann. nucl. Energy*, **16**, 1.

Alcouffe, R. (2001), PARTISN Calculations of 3D Radiation Transport Benchmarks for Simple Geometries with Void Regions, this volume of *Progress in Nuclear Energy.*

Azmy, Y. Y., Gallmeier, F. X. and Lillie, R. A., (2001), TORT Solutions for the 3D Radiation Transport Benchmarks for Simple Geometry with Void Region, this volume of *Progress in Nuclear Energy.*

Brown, P.N., Chang, B. and Hanebutte, U.R., (2001), Spherical Harmonic Solutions of the Boltzmann Transport Equation via Discrete Ordinates, this volume of *Progress in Nuclear Energy.*

Haghighat, A. and Sjoden, G.E. (2001), Effectiveness of PENTRAN^{TM}'s Unique Numerics for Simulation of the Kobayashi Benchmarks, this volume of *Progress in Nuclear Energy.*

Jung, J. et al. (1974), Numerical Solutions of Discrete-Ordinate Neutron Transport Equations Equivalent to P_L Approximation in $X - Y$ Geometry, *J. Nucl. Sci. Technol.* **11**, 231.

Kobayashi, K. (1995), On the Advantage of the Finite Fourier Transformation Method for the Solution of a Multi-group Transport Equation by the Spherical Harmonics Method, *Transp. Theory Statis. Phys.* **24**, 113.

Kobayashi, K. (1997), A Proposal for 3D Radiation Transport Benchmarks for Simple Geometries with Void Region, *3-D Deterministic Radiation Transport Computer Programs*, OECD Proceedings, p.403.

Kobayashi, K., Sugimura, N. and Nagaya, Y. (1999), 3D Radiation Transport Benchmarks for Simple Geometries with Void Region, *M & C ' 99 - Madrid, Mathematics and Computation, Reactor Physics and Environmental Analysis in Nuclear Applications*, p.657, Madrid, 27-30 September.

Konno, C. (2001), TORT Solutions with FNSUNCL3 for KOBAYASHI's 3D Benchmarks, this volume of *Progress in Nuclear Energy.*

Kosako, K. and Konno, C. (1998), FNSUNCL3 - GRTUNCL code for TORT, JAERI/Review 98-022, p. 140. See also Kosako, K. and Konno, C. (1999), FNSUNCL3: First Collision Source Code for TORT, Proc. of the Ninth International Conference on Radiation Shielding ICRS-9, Tsukuba, 17-22 October, Journal of Nuclear Science and Technology, Supplement 1, March 2000, p. 475.

Mori, T. and Nakagawa, M. (1994), *MVP/GMVP: General Purpose Monte Carlo Codes*, JAERI-Data/Code 94-007 [in Japanese].

Oliveira, C.R.E., Eaton, M.D. and Umpleby, A.P. (2001), Finite Element-Spherical Harmonics Solutions of the 3D Kobayashi Benchmarks with Ray-Tracing Void Treatment, this volume of *Progress in Nuclear Energy.*

Reed, WM. H. (1972), Spherical Harmonics Solutions of the Neutron Transport Equation from Discrete Ordinate Codes, *Nucl. Sci. Eng.* **49**, 10.

Sartori, E. (1997), Editor, *3D Deterministic Radiation Transport Computer Program. Features, Applications and Perspectives*, OECD Proceedings, Nuclear Energy Agency.

Suslov, I., (2001), Improvements in the Long Characteristics Method and Their Efficiency for Deep Penetration Calculations, this volume of *Progress in Nuclear Energy.*

Takeda, T. and Ikeda, H. (1991), *3-D Neutron Transport Benchmarks*, NEACRP-L-330.

Zmijarevic, I. and Sanchez, R. (2001), Deterministic Solutions for 3D Kobayashi Benchmarks, this volume of *Progress in Nuclear Energy.*